Comparison of Single Cell Volume Between Two-Dimensional and Three-Dimensional Cell Culture

By

Joshua Manning

B.A., Worcester Polytechnic University, 2019

A thesis submitted in partial fulfillment of the requirements for the Degree of Master of Science in the Department of Molecular Pharmacology, Physiology and Biotechnology, and the Center of Biomedical Engineering at Brown University

Providence, Rhode Island

May 2021

Declaration of Authorship

As the sole author of this thesis, I authorize Brown University to lend it to other institutions for the purpose of scholarly research.

Signed: Joshua Manning Date: 4/1/2021

Joshua Manning, Author

I further authorize Brown University to reproduce this thesis by photocopying or other means, in total or in part, at the request of other institutions or individuals for the purpose of scholarly research.

Signed: Joshua Manning Date: 4/1/2021

Joshua Manning, Author

Signature Page

This thesis by Joshua Manning is accepted in its present form by the Center of Biomedical Engineering as satisfying the thesis requirement for the degree of Master of Science.

Signed: Jeffrey Morgan Date: 4/1/2021

Dr. Jeffrey Morgan, Advisor

Signed: Blanche Ip Date: 4/1/2021

Dr. Blanche Ip, Reader

Signed: Date: 4/1/2021

Dr. Kimani Toussaint, Reader

Approved by the Graduate Council

Signed: Marissa Gray Date: 4/1/2021

Dr. Marissa Gray, Biomedical Engineering Master's Program Director

Acknowledgments

I would first like to acknowledge and thank my family for the many years of incredible support. To my parents, thank you for helping me throughout this journey and for giving me every opportunity you could to help me succeed in my endeavors. I am forever grateful for your support and your continued motivation. To Kali, thank you for helping me through all the difficult times and for mentoring me throughout my scientific career. I will always be grateful for everything you do for me, and it is always so nice to have somebody to talk science with.

I would also like to acknowledge and thank everyone within the Morgan Lab for making the past two years so enjoyable and for helping make this thesis project possible. Starting with Dr. Jeffrey Morgan, thank you for giving me the opportunity to join your lab and for your invaluable advice and mentoring over the years. To Dr. Blanche Ip, thank you for taking me under your wing and for mentoring me over the past two years. Thank you for allowing me to aid with your work and for all of the training and advice you offered to me. Thank you to the rest of the Morgan Lab both past and present, specifically Ben, Andrew, Caitlin, and Karl for your expertise and help. You have all played a significant role in making this thesis possible.

Table of Contents

List of Figures

List of Tables

Abstract

Recent advancements in the techniques used for developing *in vitro* three-dimensional cell cultures, such as bioprinting or microtissue formation, has offered a more accurate representation of *in vivo* environments when compared to two-dimensional monolayers. However, due to the advanced structure of 3D cultures, new analysis techniques are needed to assess potential physiological variations between individual cells within these constructs. Cell volume regulation has been shown to play a pivotal role in determining cell functionality both *in vivo* and *in vitro*. Cellular proliferation and apoptosis are both mechanisms regulated by cell volume. It is necessary to develop a technique for assessing cellular interactions, physiology, and morphology within the inner regions of microtissues.

The work of this thesis aims to establish an imaging technique capable of analyzing single cells within 3D microtissue environments, in order to quantify and compare single cell volume between 2D and 3D cultures. Human ovarian granulosa-like tumor cells (KGNs) were seeded within a 3D spheroidal environment using a non-adhesive agarose mold and stained at a 10% ratio using cell tracker green. Using confocal microscopy, individual cells could be distinguished within the greater microtissue construct and analyzed for cell volume. The volume of single cells within the 3D microtissue appeared to decrease when compared to cells within 2D culture environments. In addition, cells located at the interior positions of the spheroid showed lower volumes when compared to cells located at the outer regions. The results of this thesis aims to provide a high-throughput technique for observing individual cells within a microtissue construct. Having a high-throughput method will allow for assessment of physiological variations of individual cells within 3D cell culture environments.

Chapter 1

Background

1.1 Cell Volume

Mammalian cells have been shown to be more susceptible to volume changes *in vivo* due to their highly permeable plasma membrane (Mongin (2001)). During homeostasis, the cell remains in a steady-state condition, where the volume and ion concentration between the intracellular and extracellular microenvironments remain constant (Kay (2019)). Changes that occur to the volume of the cell past this steady-state condition can serve as signals for different physiological processes, including cell proliferation, apoptosis, and migration (Jiang (2013)).

The regulation of cell volume and pressure between the intracellular and extracellular environments are associated with multiple different essential elements (Jiang (2013)). These elements include both active and passive transport channels through the membrane, as well as mechanosensitive channels induced by changes in the active stresses acting on the cell (Jiang (2013)). Cells have been shown to activate these mechanisms, collectively known as either regulatory volume increase (RVI) or regulatory volume decrease (RVD), in response to changes in osmolarity and solute content between the cellular gradient (Strange (2004)).

1.1.1 Regulatory Volume Decrease

Increase in cell volume is attributed to an influx of water into the cell through changes in osmotic forces (Kay (2019)). The change is osmolarity signals the activation of regulatory volume decrease (RVD) (Mongin (2001)). The activation of the RVD pathway is significant in maintaining cellular homeostasis within the system. The mediation of RVD is controlled through the membrane transport process of the K-Cl cotransporter (Strange (2004)). The K-Cl transporter pathway regulates cell volume through mediating ion release through transport channels in the cell membrane (Lang (2007)). Activation of the K^+ and Cl^- channels signals the release of K^+ and Cl^- from the intracellular environment (Lang (2007)). The release of ions leads to a decrease in cell volume and reversal of volume measurements to those seen in steady state (Strange (2004)).

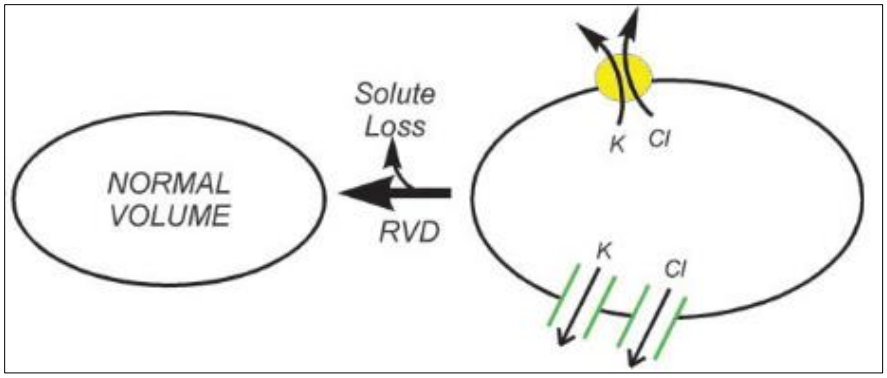

Figure 1.1: Regulatory volume decrease through activation of K-Cl transporter channel and K^+/Cl^- loss (Strange (2004)).

1.1.2 Regulatory Volume Increase

Exposure of cells to a hypertonic environment results in an osmotic flux of water through the permeable membrane and out of the cell (Burg (2008)). The transfer of water out of the cell results in cell volume shrinkage, and results in the combined activation of the Na^+/H^+ and Cl^-

/HCO_3^- exchanger (Lang (2007)). Parallel activation of the two exchangers results in Na^+/Cl^- ions being added intracellular into the system through transport channels in the membrane, while H^+/HCO_3^- ions move out of the cell (Lang (2007)).

RVI also occurs through the activation of the Na^+-K^+-$2Cl^-$ cotransporter (Lang (2007)). The cotransporter allows for the three ions to accumulate within the cell through membrane transport. The combined activation of these two pathways allows for cellular uptake of NaCl and KCl, in turn corresponding with an increase in cell volume towards normal levels (Lang (2007)).

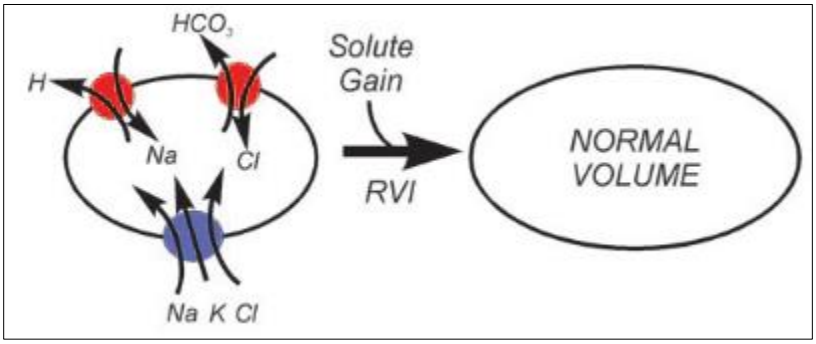

Figure 1.2: Regulatory volume increase through activation of Na^+/H^+ and Cl^-/HCO_3^- exchanger and Na^+-K^+-$2Cl^-$ cotransporter for influx of NaCl and KCl for volume increase (Strange (2004)).

1.1.3 Impact of Cell Volume on Cell Survival

Cell volume is commonly perturbed under normal physiological conditions within *in vivo* systems (Hoffman (2009)). This can be through transepithelial transport, accumulation of nutrients or metabolic waste, or through the activation of the ion transport channels discussed previously (Hoffman (2009)). Additionally, fluctuation in cell volume levels occur during pathophysiological conditions. Specifically, when hormonal function within cells is impaired, or

there is an inhibition or excess of ions passing through the plasma membrane, cells can either swell or shrink (Hoffman (2009)).

Both types of alterations of cell volume also play pivotal roles in cell survival. The mechanisms of cell proliferation and apoptosis depend on the activity of volume regulation within individual cells (Lang (2007)). Cell proliferation and cell apoptosis involve the activation of the ion transport channels required for RVI and RVD (Lang (2007)).

The activation of Cl^- channels within various types of cells leads to the loss of KCl and HCO_3^- as discussed previously. Additionally, the ion channels allow for release of osmolytes from the intracellular environment (Lang (2007)). Osmolytes allow for protein stabilization within cells, and a decrease in osmolytes from the cellular system corresponds with a destabilization of said proteins (Lang (2007)). The loss of HCO_3^- through the Cl^-/HCO_3^- exchanger has also been shown to lead to cytosolic acidification of the cell (Lang (2007)). Both protein destabilization and cytosolic acidification are concurrent with cells entering apoptosis (Lang (2007)). The unregulated cell volume decrease, called apoptotic volume decrease (AVD), and dysfunction of the RVI pathway induces apoptosis within cells both *in vivo* and *in vitro* (Maeno (2006)).

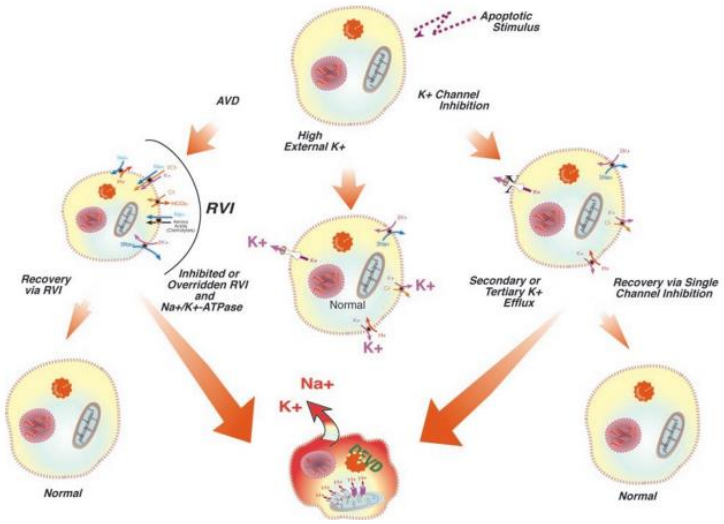

Figure 1.3: Dysfunction of RVI pathways and its effect on AVD within cells (Bortner (2002)).

Conditions which disinhibit the Na^+/H^+ exchanger and the Na^+-K^+-$2Cl^-$ pathway lead to an unregulated volume increase within cells. The accumulation of ions through these pathways into the cell associate with cell swelling as seen within RVI (Lang (2007)). The stimulation and disinhibition of these channels is caused by the depolymerization of actin filaments from the ECM (Lang (2007)). An increase in cellular volume through this pathway stimulates cell proliferation if homeostasis is not regained through RVD (Lang (2007)).

1.2 3D Microtissues

The study of three-dimensional (3D) cell culture is a technique that has been gaining popularity amongst biological researchers due to the advantages it brings towards disease modelling, tissue regeneration, and clinical testing within the pharmaceutical industry. Current drug testing protocols rely heavily on animal models prior to progressing to clinical trials. While

animal testing offers a variety of advantages for drug development, there are undeniable drawbacks which limit the effectiveness of these models. These limitations include the prominent differences in the genetics between an animal model and that of a human, in addition to the high cost of maintenance of animals (Nima, 2014).

3D cell culture has allowed for the development of *in vitro* system which closely match the characteristics of that seen within an *in vivo* human environment. Specifically, 3D culture has allowed for the development of cell-cell interactions which are absent from a two-dimensional (2D) cell monolayer (Abbott, 2003). The addition of such cell-cell interactions allows for the development of a more complex extracellular matrix (ECM) than that which can be seen in 2D (Duval, 2017). Due to these advantages, the development of new 3D cell culture techniques has been introduced involving self-assembly microtissue cultures, organ-on-a-chip, seeding with the addition scaffolds or hydrogels, and 3D cellular bioprinting (Fang, 2017).

Self-assembly microtissue cultures are a process which is scaffold-free, and more clearly mimics the processes seen within embryogenesis, morphogenesis, and organogenesis *in vivo* (Dean, 2007). The driving force behind self-assembled microtissues involves the cell-cell interactions and production of a cellular ECM resulting in an environment and matrix composition much more biologically accurate than other 3D cell culture models, such as scaffold seeding (Dean, 2007).

The Morgan lab at Brown University has developed a 3D cell culture technique via self-assembling microtissues. A micro molded non-adhesive agarose gel is developed using the 3D Petri Dish (Figure 1.4) (Leary, 2017). The polymeric mold is filled with molten agarose, which is then allowed to cool and solidify.

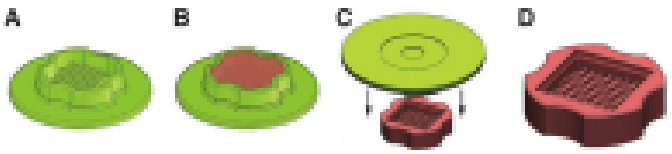

Figure 1.4: Synthesis of agarose gels using 3D Petri Dish (Leary, 2017).

Once the agarose is solidified, the mold is removed from the 3D Petri Dish and a cellular suspension is pipetted into the open area of the mold. The cells fall into the recesses through gravity and adhere to each other due to the non-adherent characteristics of the agarose gel. This allows the cells to adhere and self-assemble into a singular microtissue (Fig 1.5).

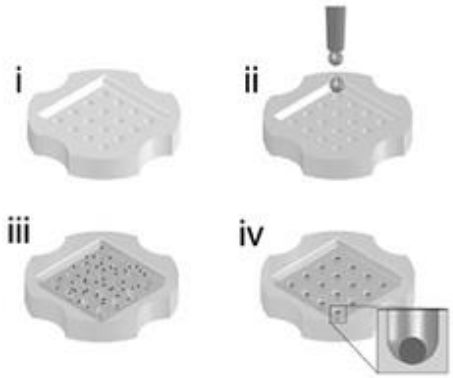

Figure 1.5: Formation of microtissues in the agarose gels via cellular self-assembly (Dean, 2007).

1.2.1 Cell Volume Variation in 3D Cell Culture

The introduction of 3D cell culture has allowed for the development of multiple cell models to attempt to mimic *in vivo* disease states. One such example is the development of 3D

spheroids synthesized using cancerous tumor cells. Such spheroids allow for the visualization of volume regulation within cancerous tumors based on environmental changes such as tonicity and extracellular compression. MCF7 breast cancer cells were cultured in inert agarose gels to form tumor spheroids. When the cells were exposed to variations of tonicity in the culture medium, there was a concurrent change in spheroid area due to RVI and RVD. By decreasing the media tonicity via hypoosmotic factors, an associated increase in spheroid area via swelling was detected. In comparison, increasing the tonicity of the culture media via hyperosmotic factors showed a significant decrease in spheroid size (Fig 1.6). (Dawson (2015))

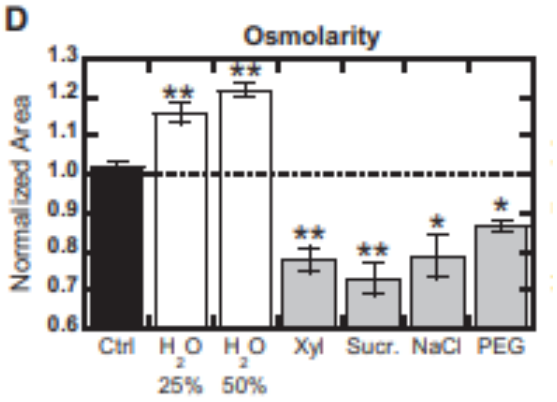

Figure 1.6: Altering the tonicity of the culture medium with hypoosmotic factors (water), or hyperosmotic factors (xylose, sucrose, NaCl, PEG) resulted in a concurrent change in spheroid area (Dawson (2015)).

Average volume of cells within three-dimensional tori synthesized with human umbilical vein endothelial cells (HUVEC) has also previously been calculated at multiple seeding densities. Tori seeded at 50K and 100K cells were left undisturbed for 20 hours. Quantification of total toroid volume was calculated via the standard equation for an ellipse, $V=(\pi hr)(2\pi R)$, where height (h), minor radius (r), and major radius (R) of the toroid were used. The experimental toroid volume was calculated at T=0 and T=20 at each seeding density to

determine the change in toroid volume over time. Both seeding densities showed a significant decrease in toroid volume over the time span (Fig 1.7). (Kanellias (2019))

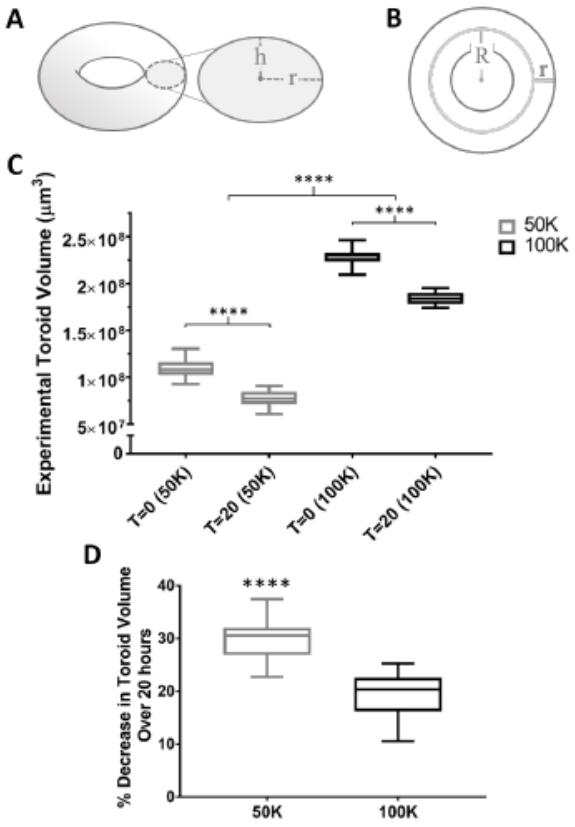

Figure 1.7: Experimental volume of HUVEC tori over 20-hour time frame. Toroid volume at 50K and 100K seeding densities were compared. A significant volume decrease within each of the seeding groups was seen. The percent decrease in 50K toroid volume was significantly more than 100K seeding group. (Kanellias (2019)).

In addition, calculations were performed to determine whether the volume decrease within the multiple seeding densities was proportional to the number of cells within the microtissue. This measurement was estimated via dividing microtissue volume by total cells within the toroid. The total tori volume at both T=0 and T=20 was divided by the total cell number in both groups. Both seeding densities showed a decrease in experimental volume per

cell over the 20-hour time period. However, the single cell volume within the 50K seeding density group decreased significantly more. (Kanellias (2019)).

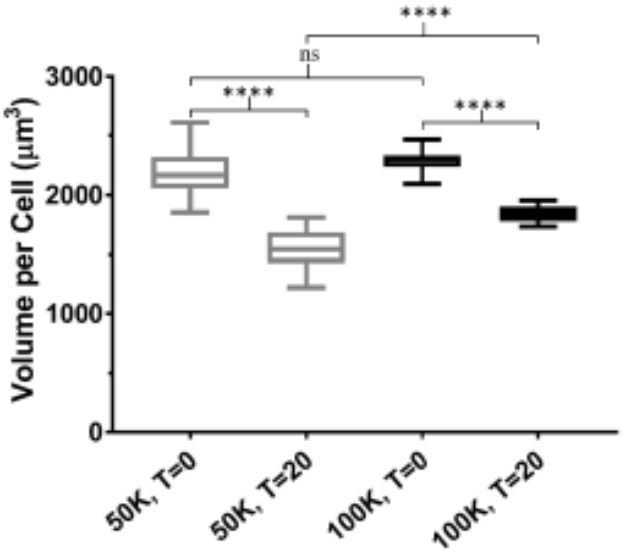

Figure 1.8: Experimental volume per cell within HUVEC tori decreases over a time interval of 20 hours. Volume per cell was calculated by dividing the total number of cells per toroid by the experimental toroid volume at both T=0 and T=20. A significant decrease in cellular volume was seen at both seeding densities over time. (Kanellias (2019)).

Mechano-osmotic models have been established in order to investigate the effects of various dynamics on cell volume within 3D microtissue environments. Specifically, models have been invoked to show how cell volume may vary depending on position within the 3D spheroid environment. Simulated cancer organoid models have been established to present how ion transport, active stresses, and osmotic differences throughout the interior of the spheroid can affect the single cell volume. (Shenoy (2020))

Solid growth stresses are present within 3D cellular microenvironments due to the proliferation of cells within the spheroid, cellular confinement, and matrix fiber tension between the cells. The solid growth stress has been shown to vary in magnitude throughout the structure,

with increased levels of stress present towards the core of the organoid. The increased level of solid growth stress within the interior of the spheroid subsequently affects the rate of ion transport between the cells. The higher stress levels close the mechanosensitive channels responsible to ion transport related to volume homeostasis. Therefore, the cells found the in core of the spheroid are more likely to have lower cellular volumes compared to those cells which are found on the outer regions of the spheroid, where there is less active stress being applied to the cells (Fig 1.9). (Shenoy (2020))

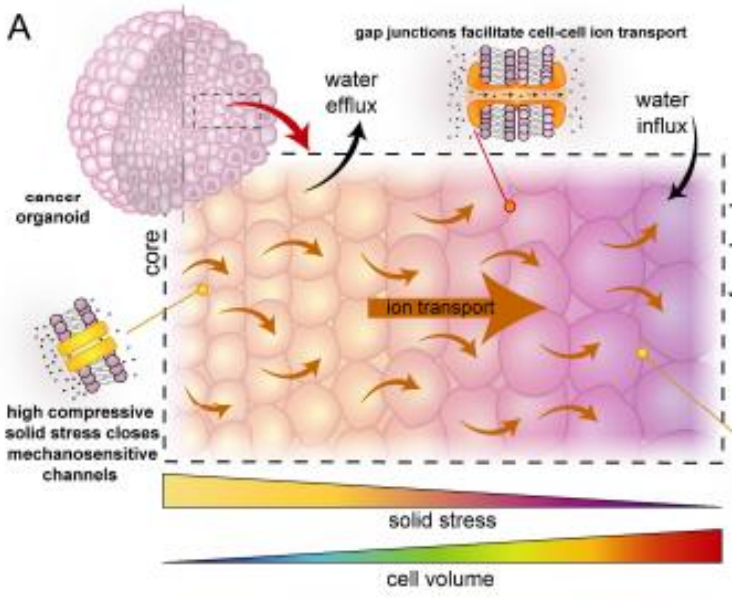

Figure 1.9: Model of a cancer organoid and the effect of solid stress on single cell volume. Positions closer to the core of the spheroid exhibit higher areas of solid growth stress on the cells. The increased stress closes channels necessary for volume homeostasis, and the cells exhibit lower volume levels than those in the outer positions (Shenoy (2020)).

Alterations in the mechanical properties of individual cells due to variations in their local environments could additionally play a role in determining overall cellular function. Reduction in cell volume consistent with that hypothesized in 3D microtissues could lead to changes in other cellular mechanics. Reduction in cell volume has been associated with increased cell

stiffness (Guo (2017)). In addition, impacts on the folding and transport of proteins within the cell, and the condensation of chromatin has been shown with decreasing cellular volume (Guo (2017)).

With respect to mesenchymal stem cells (MSCs), variation in volume has shown to affect the rate of osteogenesis within 3D culture environments. MSCs in hydrogels which stimulate volume expansion have seen enhanced osteogenesis, whereas volume reduction has been shown to cause an opposite effect, resulting in diminished osteogenesis, independent of cellular morphology (Lee (2019)). Therefore, the assessment of varying cell volume within a microtissue environment could offer further evaluation on the functionality of cells within a microtissue construct and offer an idea on the physiological accuracy of *in vitro* microtissue constructs in comparison to *in vivo* environments.

1.3 Live Cell Staining

The processes of staining live cell lines in both 2D and 3D microenvironments have expanded within the recent years. Multiple sub-categories of staining options are present for various microscopy techniques and analysis. These categories include cytoplasmic labelling, membrane labelling, and fluorescent protein labelling. The advantages and disadvantages of each staining option has been weighed for the purposes of 3D live cell analysis.

Cell Tracker staining is a membrane permeable dye used for labeling the cytoplasm of live cells. The stain remains fluorescent for at least 72 hours after loading. Cell Tracker stain is easy to use, with a loading time of thirty minutes. There is a wide excitation and emission spectrum available, with 8 different spectra. The stain is moderately resistant to photobleaching and has

little cytotoxic effects. Due to the cytoplasmic labeling mechanism, the stain allows for an even signal distribution throughout the cell.

Cell Tracker stains have already been successfully used to image cells within a spheroid. Three dimensional cellular spheroids were labeled with four Cell Tracker fluorescent stains and imaged using confocal microscopy. Imaging was used to determine the potential limitations of imaging live cell spheroids with confocal microscopy. Spheroids were labelled with Cell Tracker red, green, violet, and purple, and imaged using an Opera Phenix confocal microscope. (Leary (2018))

Cell Tracker stains were successful in the ability to label and image spheroids using the confocal microscope. One limitation that was presented dealt with the loss of fluorescent signaling using confocal imaging and its relation to z depth. There was an observed association between increasing spheroid radii and loss of fluorescent signaling. (Leary (2018))

QTracker Cell Labeling is another option for live cell cytoplasm labeling. This protocol utilizes a peptide target which delivers nanocrystals through the membrane. Similar to Cell Tracker, this comes with an option of 8 different spectra. Qtracker nanocrystals remain fluorescently stable for 6 to 10 generations within the cells, making them more durable than Cell Tracker. Fluorescence of the nanocrystals are maintained regardless of changes in pH, temperature, or metabolic activity and is also resistant to photobleaching. However, this requires a longer loading time and less even labeling within the cytoplasm due to the use of nanocrystals. QTracker cell labeling has been used to stain and track cellular proliferation in 3D microfluidic hydrogels (Knowlton (2016)).

ViaFluor SE Cell Proliferation dyes are applicable for staining the cytoplasm of viable cells. The stain covalently labels proteins throughout the inside of the cell and are non-fluorescent unless they enter viable cells. The durability of the stain can last up to several weeks and is therefore useful for long-term cell labeling. However, due to the mechanism of covalent binding, the fluorescent stain is not uniform throughout the cell. ViaFluor cells have been used in literature to measure cell proliferation through analysis with flow cytometry. This technique has been used to measure tumorigenesis in cancer cells (Showalter (2020)).

Calcein AM is a cytoplasm label which follows a similar mechanism to the ViaFluor dye, except Calcein does not utilize covalent labeling. Due to this fact, this label offers a more uniform intracellular staining than that seen with the ViaFluor. The durability of this stain after loading is less than 24 hours, making it unusable for long term testing. Calcein AM has been used to determine cellular viability and offers a method for detecting apoptosis within adherent cells (Gatti (1998)).

Table 1.1: Live cell staining techniques for cytoplasmic labelling

Market Name	Chemical Name	Ex/Em (nm)	Durability	Advantages	Disadvantages
Cell Tracker	Lipophilic carbocyanine membrane dye	353/466 371/464 415/516 492/517 548/576 553/570 577/602 630/650	-3 to 6 generations -72 hours	-Quick loading time -Moderate resistance to photobleaching -Even signal distribution throughout the cell -Applicable for antibody combination staining -Does not pass to neighboring cells	-Difficult to resolve single cells within larger spheroid
QTracker Cell Labelling	QDot Nanocrystals in borate buffer and PBS	485/525 525/565 545/585 565/605 585/625 615/655 665/705 760/800	-6 to 10 generations -Nanocrystals inherited by daughter crystals for 6 generations	-Delivered through specific enzyme so there has been no cell-type specificity seen -Fluorescence maintained regardless of changes in pH, temperature, and metabolic activity -Little cytotoxicity -Resistance to photobleaching	-Requires longer loading and targeting peptide for labelling -Uneven labeling due to use of nanocrystals
ViaFluor SE Cell Proliferation Dyes	-N/A	408/452 493/532 495/519	Wide range (days to weeks)	-Used for long-term cell labelling	-Fluorescent staining is not uniform in intracellular labelling
Calcein AM	$C_{46}H_{46}N_2O_{23}$	495/515	-Less than 24 hours	-Offers a more uniform intracellular staining	-Short term durability

PKH and CellVue Claret Fluorescent Cell Linker Dyes stain the lipid bilayer of live cells through the use of an aliphatic reporter molecule and fluorochromes. There are less emission spectra options for this stain, with only red and green spectrum available. The stains remain fluorescent for up to a month and is ideal for cell tracking and cell-to-cell interaction. The stain has successfully labeled SMCs, fibroblasts, and endothelial cells. One disadvantage is the ease of loading. The protocol requires a hypoosmotic labeling step, making it a more challenging protocol than the Cell Tracker or QTracker options. PKH staining has successfully been used to

stain and image cells within a microscaffold based cellular construct. The use of the stain was to determine the effectiveness of coculturing 4 cell types within the microscaffold (Tan (2016)).

Lectin Conjugates offer the widest selection of emission spectra due to the multiple conjugation techniques. CF labeled WGA, ConA, or PNA binds to sugar molecules on the cell membrane for short term fluorescent imaging. The stain is cell dependent and does not allow permeabilization within the cell unless fixed. However, there has been shown to be a large amount of dye transfer between cells, higher toxicity, and varied effectiveness based on cell type. For this reason, lectin conjugate staining is primarily used for drug testing between potential targets and live cells and would not be applicable for use in this project (Wirth (2002)).

BioTracker Cytoplasmic Membrane Dye labels the plasma membrane through insertion within the lipid bilayer, and also permeabilizes over time through incorporation into endocytic vesicles. The stain lasts on average several weeks; however, this varies with cell type. The stain offers little dye transfer between cells and has low toxicity levels. However, due to the permeabilization via endocytic vesicles, it offers uneven intracellular staining. The BioTracker dye has been used successfully to label and track stem cells within a 3D scaffold or biomaterial. In addition, the dye has been utilized to track stem cells within *in vivo* tissue models (Chikate (2019)).

Octadecyl Rhodamine B Chloride (R18) is applicable for labelling the plasma membrane of cells for use in both 2D and 3D microscopy. It is a lipophilic structure, with the fluorophore present at the aqueous interface of the membrane and the tail inserting into the lipid level. The stain has been utilized with confocal microscopy to analyze cell volume variation of mesenchymal stem cells (MSC) within hydrogels under varying osmotic pressure (Chaudhuri (2019)).

Table 1.2: Live cell staining techniques for plasma membrane labelling

Market Name	Chemical Name	Ex/Em (nm)	Durability	Advantages	Disadvantages
PKH and CellVue Claret Fluorescent Cell Linker Dyes	-Incorporates aliphatic reporter molecules and fluorochromes	490/504 551/567 655/675	-Long lasting -Month long tracking	-Successfully labelled SMCs, fibroblasts, endothelial cells -Ideal for cell tracking and cell-to-cell interaction	-Requires hypoosmotic labelling protocol
Lectin Conjugates: ConA	Concanavalin A	347/448 404/431 408/452 490/515 593/614 630/650 642/662 681/698 755/777 770/797	-Short term durability	-No permeabilization unless fixed before staining -Cell dependent	-Dye transfer between cells -Higher toxicity -Effectiveness varies between cell types
Lectin Conjugates: WGA	Wheat Germ Agglutinin	347/448 404/431 408/452 490/515 527/558 555/565 562/583 593/614 630/650 642/662 681/698 680/701 770/797	-Short term durability	-No permeabilization unless fixed before staining -Cell dependent	-Dye transfer between cells -Higher toxicity -Effectiveness varies between cell types
Lectin Conjugates: PNA	Arachis hypogaea CF Dyes	490/515 562/583 593/614 642/662	-Short term durability	-No permeabilization unless fixed before staining -Cell dependent	-Dye transfer between cells -Higher toxicity -Effectiveness varies between cell types
BioTracker Membrane Dye	Lipophilic carbocyanine membrane dye	336/441 484/501 549/565 644/665 767/806	-On average several weeks -Varies with cell type	-Can stain both adherent cells and cells in suspension -Little dye transfer -Low toxicity	-Permeabilize over time -Uneven live cell staining
Invitrogen R18	Octadecyl Rhodamine B Chloride	556/580	-Short term durability	-Previously used to stain cellular spheroids -Capable of being imaged with confocal microscopy	-Limited information on staining effects and permeability

BacMam Transduction Control is a cell tracking technique which utilizes fluorescent proteins. These proteins transduce intracellularly with a technology similar to that of an insect virus. The stain remains durable from 5 days to 2 weeks. This allows for easy cellular tracking, however there is a wide range of expression since on average only 90% of cells will express the protein. Past studies have used this viral transduction method to determine protein expression within mammalian cells, and not for cell tracking or cellular interactions (Kato (2016)).

Table 1.3: Fluorescent protein live cell tracking

Market Name	Chemical Name	Ex/Em (nm)	Durability	Advantages	Disadvantages
Cell Tracking with Fluorescent Proteins (Thermo-Fisher)	BacMam GFP Transduction Control	488/510	-5 days to 2 weeks	-Allows for easy tracking of cells -Can target specific subcellular structures	-Only 90% of cells express the protein -Wide range of expression as a result
Cell Tracking with Fluorescent Proteins (Thermo-Fisher)	Red Fluorescent Protein (RFP)	488,532/588	-5 days to 2 weeks	-Can target specific subcellular structures -Minimal toxicity and cellular disruption	-Less than 100% transfection rate -Rates vary per cell type
Cell Tracking with Fluorescent Proteins (Thermo-Fisher)	Plasma Membrane-Cyan Fluorescent Protein	435/485	-5 days to 2 weeks	-Easy labelling technique for plasma membrane -Can use multiple tracking dyes alongside CFP	-Less than 100% transfection rate -Rates vary per cell type

1.4 Three-Dimensional Imaging Techniques

With the expanding development of *in vitro* microtissue models, there is a concurrent need for efficient imaging and analysis within the 3D environment. Specifically, imaging techniques which allow for tissue penetration within these thicker tissue models are required. Previously, the

method for imaging internal structures of 3D models resulted in microtissue sectioning or histology, neither of which are suitable for live cell imaging (Hoffman-Kim (2015)). However, advancements in varying microscopy techniques have allowed the assessment of internal microtissue structures. Specifically, Confocal Microscopy (CM), Light-Sheet Microscopy (LSM), and Multiphoton Microscopy (MPM) are three-dimensional techniques applicable for imaging live cell microtissues.

1.4.1 Confocal Microscopy

Confocal microscopy (CM) denotes an accepted widespread field utilized for three-dimensional imaging of living samples (Jonkman (2015)). CM offers the ability to generate high-contrast images via the use of optical sectioning (Mura (2019)). Optical sections can be generated at values thinner than 1 µm without the need of physically sectioning the sample (Jonkman (2020)). In addition, CM is able to reject out-of-focus light and background to allow for clear optical imaging of the biological sample (Mura (2019)).

CM utilizes a laser light as the point illumination source for imaging the sample. The illumination point moves across the sample at different z heights to obtain optical sections or z-stacks (Alvarez-Roman (2004)). The z-stacks are then combined to form a single three-dimensional image of the sample. Out-of-focus light is filtered out of the system via the use of an aperture. The pinhole only allows light within the focal plane to pass through to the detector, decreasing the presence of background noise during image acquisition (Fig 1.10) (Hovis (2010)).

However, during image acquisition the entirety of the sample is illuminated via the laser. This can result in increased photobleaching within the sample and limits the exposure time of the

live sample within the system (Alvarez-Roman (2004)). Additionally, while the aperture is able to decrease background light during image acquisition, the presence of light scattering within the system limits the penetration depth when imaging larger tissues (Leary (2018)).

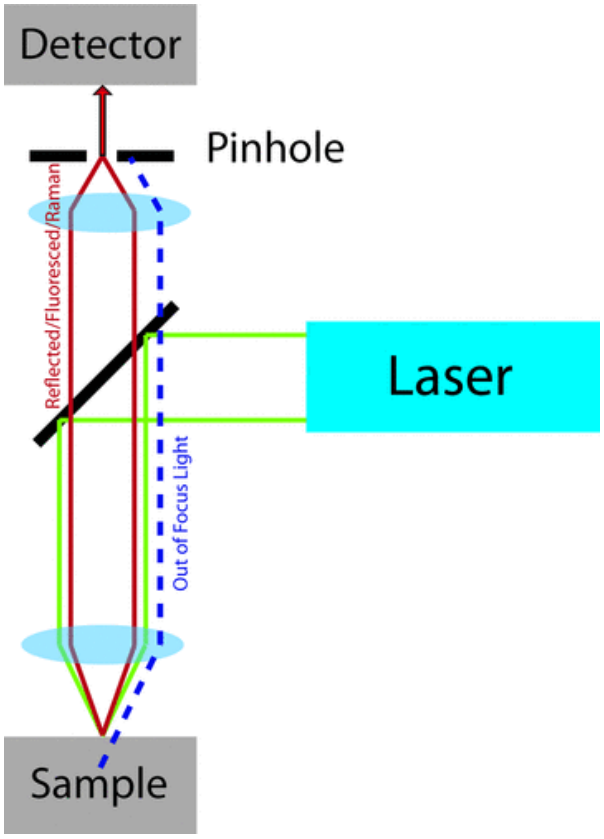

Figure 1.10: Optical path schematic of a confocal microscope. The sample is illuminated via the use of a laser. The presence of the pinhole allows for the rejection of out-of-focus light being acquired from the detector, resulting in clear optical imaging of the sample.

1.4.2 Light-Sheet Microscopy

LSM is a form of microscopy which functions as a non-destructive imaging technique capable of imaging living tissues in a three-dimensional environment (Santi (2011)). The technique provides high imaging speed with a high signal-to-noise ratio and low levels of photobleaching, causing it to have low phototoxic effects on living specimens (Keller (2012)).

LSM utilizes a thin plane of light to section living tissues labeled with a fluorophore (Santi (2011)). Unlike other forms of three-dimensional microscopy, the tissues being imaged are only subjected to a single plane of light, instead of the entire tissue being illuminated evenly at one time (Weber (2014)). This significantly decreases the probability of photobleaching and phototoxicity of the specimen being imaged allowing for living samples to be imaged over longer periods of time when compared to other imaging techniques (Weber (2014)).

In addition, the light plane in LSM allows for optical sectioning of the tissue to be achieved across the total field of view in a single exposure time (Weber (2014)). This allows for quicker image analysis of samples when compared to other imaging techniques (Weber (2014)). The lateral resolution of LSM is approximately equal to that seen in wide-field and confocal microscopy, however LSM offers a two-fold increase in lateral resolution when compared to CM (Weber (2014)).

However, while the imaging time using the LSM is significantly shorter when compared to other techniques, the sample preparation and alignment within the system is more time consuming. LSM combines two separate objectives within the system (Fig. 1.11). The detection objective is positioned to allow for detection of the focal plane used for image analysis, while the illumination objective is used to illuminate the sample with the light sheet (Weber (2014)). These objectives are perpendicular to each other within the system, and therefore makes it difficult to align both objective paths within the focal space (Santi (2011)). This can create focus issues when imaging the sample and increases setup time prior to imaging.

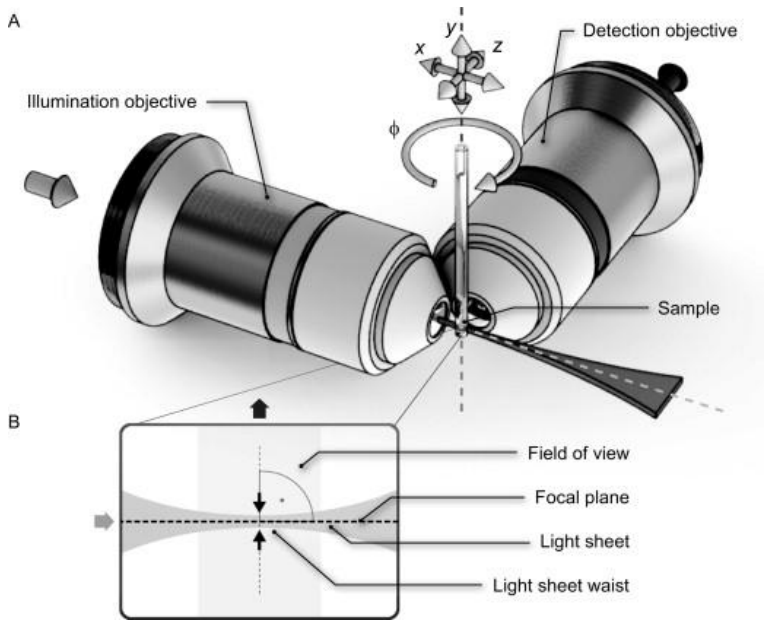

Figure 1.11: Sample schematic of dual-objective LSM setup. The detection and illumination objectives are positioned perpendicular to each other. The sample is positioned at the intersection of the objective focal planes and imaged via a single plane of light illuminated from the illumination objective (Weber (2014)).

1.4.3 Multiphoton Microscopy

Two-photon excitation microscopy is the most commonly used MPM imaging application when dealing with biological samples (Ustione (2011)). This imaging technique has been used in live cell imaging due to its increased penetration depth within the sample and decreased out-of-focus bleaching during image acquisition when compared to CM (Tauer (2004)).

MPM employs near infrared (NIR) lasers to generate nonlinear signals within the visible light spectrum (Larson (2010)). MPM utilizes the idea of multiphoton excitation within a biological tissue. This occurs when two photons simultaneously reach the desired sample and promotes the desired fluorophore from its ground state to its excited state (Fig 1.12) (Larson (2010)). The two photons contain the necessary transition energy to promote the fluorophore to its excited state needed for fluorescent imaging of the sample (Larson (2010)). This imaging

technique can be utilized with both exogenous fluorescent probes and stains, as well as endogenous probes such as transfected fluorescent proteins (Larson (2010)).

The NIR excitation is restricted to a small portion of the sample, allowing for the technique to be completed without the need of an aperture (Tauer (2004)). Additionally, the NIR can penetrate at deeper tissue depths than seen in CM and with reduced light scattering, eliminating background noise and bleaching (Williams (2001)).

One limitation presented with this technique is the increased potential of photobleaching within the excitation focal plane (Tauer (2002)). The NIR excitation via the two photons can increase the photobleaching rate within the focal volume section of the tissue being imaged when compared to LSM an CM (Ustione (2011)).

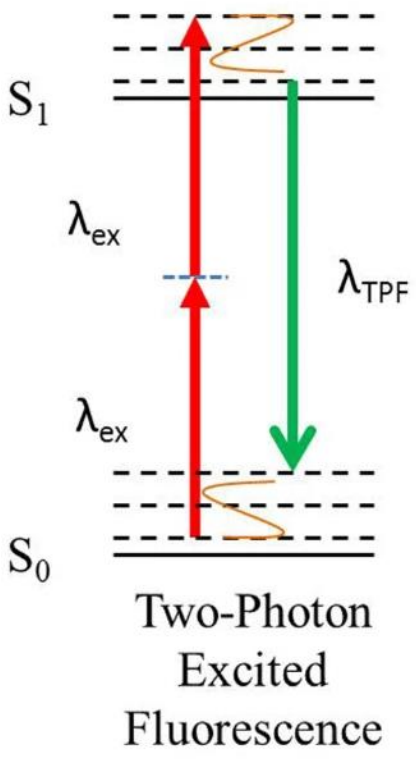

Figure 1.12: Jablonski diagram depicting the excitation and relaxation of fluorophores within MPM. Red arrow depicts the two NIR photons simultaneously reaching the fluorophore, causing it to increase to its excited state. The green arrow indicates the visible fluorescence acquired during relaxation of the fluorophore (Larson (2010)).

1.4.4 Comparison of Three-Dimensional Imaging Techniques

The three microscopy techniques previously described are accepted across the biological field for imaging three-dimensional biological samples. Confocal microscopy allows for the acquisition of high-contrast three-dimensional images via optical sectioning. Illumination of the sample via a laser allows for optical sections as low as 1 μm to be acquired. The presence of an aperture allows for the removal of out-of-focus light to be detected within the focal plane to allow for clear optical images of the sample. However, the risk of photobleaching and limited penetration depth within thicker tissues provide limitations for this type of technique.

Light sheet microscopy allows for the acquisition of optical sections similar to that of CM. However, in this technique, only the focal plane is illuminated within the sample. This decreases the chance of photobleaching of the sample and allows for imaging over longer time points. The lateral resolution capable of being imaged using LSM is also greater than that seen within CM. However, the sample preparation due to the dual-objective format within the LSM causes an increased difficulty and time constraint in sample loading.

The multiphoton technique allows for an increased penetration depth within larger tissues and decreases background bleaching due to its compacted focal plane. This offers clearer image quality and the ability to image tissues with greater areas. However, this technique results in an increased potential for photobleaching within the focal region due to the two-photon excitation.

Based on the advantages and limitations presented between the different techniques, as well as time limitations and accessibility, the Opera Phenix High Content Screening confocal microscope will be used for this study. The Opera Phenix allows for increased sampling times compared to other forms of CM and has been previously used in imaging three-dimensional microtissues.

Three-dimensional cell culture has offered a more accurate representation of *in vivo* environments when compared to 2D culture, due to the addition of the added dimension. However, new analysis techniques are required for assessing potential physiological variations and cellular interactions occurring between individual cells within the microtissue construct. Three-dimensional volume analysis using the Opera Phenix High Content Screening System could allow for a technique to observe and quantify single cell volume within a greater microtissue construction. Previous experiments have suggested that there has been a significant decrease in theoretical volume per cell within the greater microtissue construction (Fig 1.8). By

quantifying individual cell volume within spheroidal microtissues, we hypothesize that the volume of a single cell will be less than that seen within two-dimensional culture environments.

Table 1.4: Comparison of three-dimensional microscopy techniques utilized for live cell imaging

	Multiphoton	**Confocal**	**Light Sheet Microscopy**
Advantages	- Increased depth penetration within larger tissues - Decreases background bleaching due to compacted focal plane	- Acquisition of high-contrast three-dimensional images via optical sectioning - Removal of out-of-focus light via aperture	- Minimizes exposure of entire sample to light (decreased photobleaching and phototoxicity) - Enables imaging over longer period - Greater lateral resolution
Disadvantages	- Increased potential for photobleaching within the focal region	- Produces photobleaching and phototoxicity due to large excitation energy and illumination of entire sample - Limited penetration depth of thicker tissues	- Sample preparation due to dual-objective format causes an increased difficulty and time constraint during sample loading

Chapter 2

Materials and Methods

2.1 Cell Culture

KGN cells were grown and expanded in a solution containing Dulbecco's Modified Eagle Media 1X (DMEM)(Gibco), 10% Fetal Bovine Serum (FBS)(Gibco), and 1% penicillin/streptomycin (P/S)(MP Biomedicals). Cells were incubated at 37˚C and 5% carbon dioxide (CO_2). Cell media was replaced every 72 hours until the T-75 flask was confluent. Upon confluency, the cells were washed with PBS prior to trypsinization at a 0.05% concentration. Cells were incubated with trypsin at 37˚C and 5% CO_2 for 5-8 minutes. The trypsin solution was deactivated by quenching with culture media and transferred to a 50mL conical tube. Cells were centrifuged at 800 rpm for 6 minutes. The quenched media was aspirated, and cells were resuspended in serum free media for counting and seeding.

2.2 KGN Fluorescent Staining

For two-dimensional cell staining, KGN cells were stained with a 5 µM Cell Tracker Green (CMFDA)(Thermo Fisher Scientific, Waltham, MA) staining solution. The 5 µM CMFDA staining solution was prepared by adding 5 µL CMFDA to 10 mL of serum-free cell media. The excitation spectrum for CMFDA is 546/568nm. Prior to cell passaging, the staining solution was added to KGN cells in a T-75 flask and incubated for 30 minutes. The staining

solution was aspirated from the flask following the incubation time and 10mL of fresh serum-free media was added to the cells for an additional 30 minutes. Following this second incubation time, the serum-free media was aspirated, and the cell culture protocol proceeded as previously stated.

For three-dimensional imaging, a portion of KGN cells were stained with 5 µM Cell Tracker Green (CMFDA)(Thermo Fisher Scientific, Waltham, Ma). A staining solution with 5µM CMFDA in serum-free media was prepared by adding 5µL of CMFDA to 10mL of serum-free media. Prior to cell passaging, the staining solution was added to one flask of cells and followed the protocol stated above with 2D staining.

For three-dimensional nuclear staining, KGN cells were stained with a 1:2000 part Hoechst 33342 (Thermo Fisher Scientific, Waltham, Ma) staining solution. A staining solution was prepared by adding 5µL of Hoechst to 10mL of serum-free media. Prior to cell passaging the staining solution was added to one T-75 flask containing KGN cells and incubated for 30 minutes. The staining solution was aspirated following the incubation time and 10mL of fresh serum-free media was added to the cells for an additional 30 minutes. The serum-free media was then aspirated, and the cell culture protocol was completed on the stained cells.

2.3 Creation of Hydrogel Molds

Polymeric 3D Petri Dish® spheroid micro-molds (Microtissues Inc., Providence, RI) and agarose (Fisher Bioreagents) were sterilized using an autoclave. A 2% agarose solution was synthesized by adding sterile water in the appropriate weight/volume ratio. The agarose solution was heated until clear and homogenous, and then pipetted into the spheroid micro-molds. The

agarose gel was allowed to solidify before being removed from the micro-mold and transferred into 12-well plates. The gels were equilibrated by adding 2 mL of serum-free media per well and incubated overnight.

To evaluate two-dimensional trypsinized cells, a 2% agarose solution was created per the above protocol. Molten agarose was added to each well of a CellView 96-well plate (Greiner Bio-one), covering the bottom of the well, and allowed to solidify. This created a non-adherent surface for the cells to be seeded on. After solidifying, the well was equilibrated via overnight incubation in serum-free media prior to cell seeding.

2.4 KGN Seeding Within Different Culture Environments

For measuring 2D adhered cell volumes, a 10% CMFDA KGN cell suspension created using the protocol described previously was seeded at a density of 50K cells per well within a CellView 96 well glass bottom plate. The confluent cell cultures were trypsinized and counted to obtain the desired density for seeding within the wells. The cells were allowed to adhere to the plate via an overnight incubation period prior to confocal imaging.

2D trypsinized volumes were measured using a 10% CMFDA KGN cell suspension seeded at a density of 50K cells per well within the agarose coated 96 well plate. The agarose coated 96 well plate was created via the procedure described previously. The confluent KGN cells were then trypsinized and counted to obtain the desired seeding density for seeding within the agarose coated wells. The cells were seeded within the agarose coated wells and incubated overnight prior to confocal imaging.

Spheroid microtissues were formed following gel equilibration. Both CMFDA stained and unstained KGN cells were trypsinized, counted, and resuspended to the appropriate cell density required for seeding. The resuspension included 10% KGN cells stained with CMFDA, and 90% unstained KGN cells. The cell suspension was then pipetted into the center of each mold and the plates were subsequently incubated for 30 minutes in media to allow for self-assembly of the spheroids. Following the 30-minute incubation time, 2 mL of media was added to the wells containing the molds and the spheroids were incubated overnight. The spheroids were released from the 3D Petri Dish® after the overnight incubation by gently pipetting with a P1000 pipette until the spheroids were loose in the media. The spheroids were then transferred from the molds to a CellView 96 well plate and imaged using the Opera Phenix.

2.5 Acquisition of Confocal Imaging

Two-dimensional cell culture environments were imaged using confocal microscopy via the Opera-Phenix High Content Screening System (PerkinElmer). The Opera-Phenix microscope allowed for imaging 3D stacks using a 20x water immersion objective (NA = 1). The 3D image stacks of the KGN cells were obtained using a 1µm z-axis interval. A total height of 50 µm was imaged within each sample well.

Three-dimensional spheroids were also imaged using the Opera-Phenix system. The Opera-Phenix microscope allowed for imaging using 3D stacks using a 40x water immersion objective (NA = 1.1). The 3D image stacks of the KGN spheroids were once again obtained using a 1µm z-axis interval. A total height of 250µm was imaged within each sample well to allow for imaging of the entire height of the spheroids.

2.6 Cell Volume Analysis

Cell volume measurements of the 2D cell culture environments and 3D spheroids were calculated using the Harmony software. Region of interest (ROI) attachments from the Harmony software were utilized for distinguishing individual cells, and subsequent volume measurements. Two-dimensional adhered cells were analyzed using the Find Nuclei ROI attachment. ROIs were automated on the individual adhered cells, and the Harmony software automatically calculated the volume measurements throughout the height of the z-stack.

Two-dimensional non-adhered cells were analyzed using the Find Nuclei ROI attachment included with Harmony. Individual ROIs were automated around individual cells throughout the height of the z-stack and volume measurements were calculated via the Harmony software.

Single cells within a three-dimensional spheroid were also analyzed via the Find Nuclei ROI attachment. ROIs were automated around cells throughout the entirety of the spheroid, and volume measurements were once again calculated via the Harmony software.

The volume datasets obtained from the three conditions were filtered to eliminate measurements from single ROIs containing multiple cells and ROIs containing staining segments not quantitative of a single cell. Volume measurements greater than 7000 μm^3 were excluded from analysis to eliminate multiple cell ROIs measured via the Harmony software. Volume measurements less than 1000 μm^3 were excluded from data analysis as well. On average, ROIs formed below this parameter contained stained segments within the field of view and were not connotative of a single cell.

Significance between environmental conditions were tested using the JMP Pro 15 statistical software. Normality of the data was performed via the Shapiro-Wilk Goodness-of-Fit

test ($p < .05$). Comparison across the three conditions was performed using a One-Way ANOVA ($p < .05$), with further comparison using the Tukey multiple comparison test ($p < .05$).

Volume evaluation between varying positions within the microtissue was performed via the Harmony software. Cells located on the exterior surface of the spheroid were measured between each biological sample. Cells located within the interior of the spheroid was denoted as cells positioned greater than 20 µm from the surface of the spheroid towards the interior of the spheroid. Normality of the data was performed via the Shapiro-Wilk Goodness-of-Fit test ($p < .05$). Significance between the volume measurements at different positions was measured using a two-tailed, unpaired t-test with Welch's correction ($p < .05$).

Chapter 3

Analysis of Cell Volume in Two-Dimensional Culture

3.1 Cell Volume Analysis Using Opera Phenix

Quantification of four different environments was conducted to determine single cell volume between two-dimensional culture environments, and three-dimensional cell environments. To evaluate the accuracy of cell volume analysis using the Harmony software, microparticles of a known size were used as a control. A CellView 96 well glass bottom plate was seeded at a density of 1000 microparticles per well and imaged using the Opera Phenix (Fig 3.1). Volume analysis of the microparticles was conducted using the Harmony software, and the average volume measurements was compared to the known volume of the microparticles.

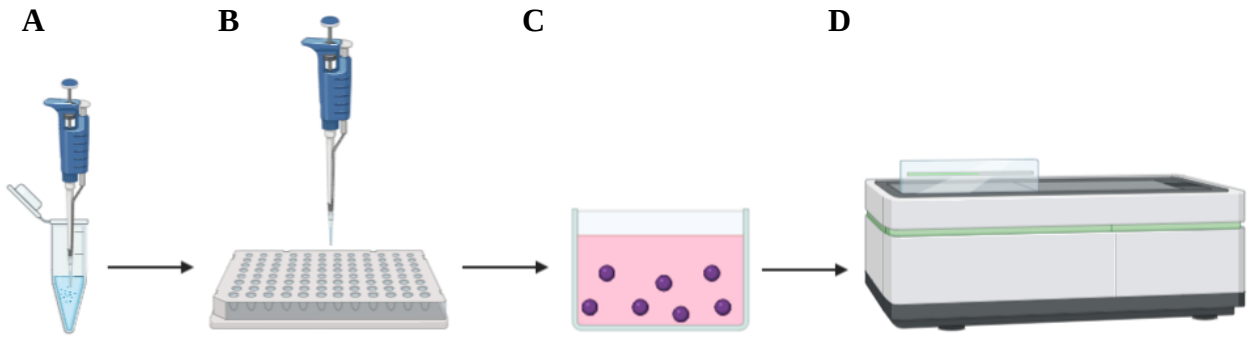

Figure 3.1 Confocal imaging of Polyscience Violet Microbeads. (A) A set volume of microbeads is suspended in PBS. (B) The microbeads suspension is seeded within a CellView 96

well glass bottom plate at a density of 1000 beads/well. The microbeads are allowed to settle to the bottom of the well (C) and imaged using the Opera Phenix (D).

In order to assess the accuracy of the volume analysis using the Opera Phenix, the known volume distribution of the microbeads was calculated. Per Polysciences, the microbeads had a mean diameter of 10.647 $\pm$ .975µm. Given the spherical nature of the microparticles, it can be assumed that the volume for a sphere equation can be utilized for control calculation measurements. Using these parameters, the known volume distribution of the microbeads within three standard deviations can be calculated using the following equation.

$$Vsphere = \frac{4}{3}\pi r^3$$

To determine the experimental volume measurements using the Opera Phenix, microbeads were imaged at z-stacks of 1µm for a total height of 35µm to ensure imaging of the entire microbead. The Find Nuclei analysis tool from the Harmony software quantified volume measurements of individual microbeads across the z-height (Fig 3.2). The mean experimental volume measurements were then compared to the known volume measurements calculated previously (Fig. 3.3). The average experimental volume calculated using the Opera Phenix was found to be 670.9 $\pm$ 185.3µm^3, whereas the known volume of the microbeads was 631.9 $\pm$ 174.1µm^3.

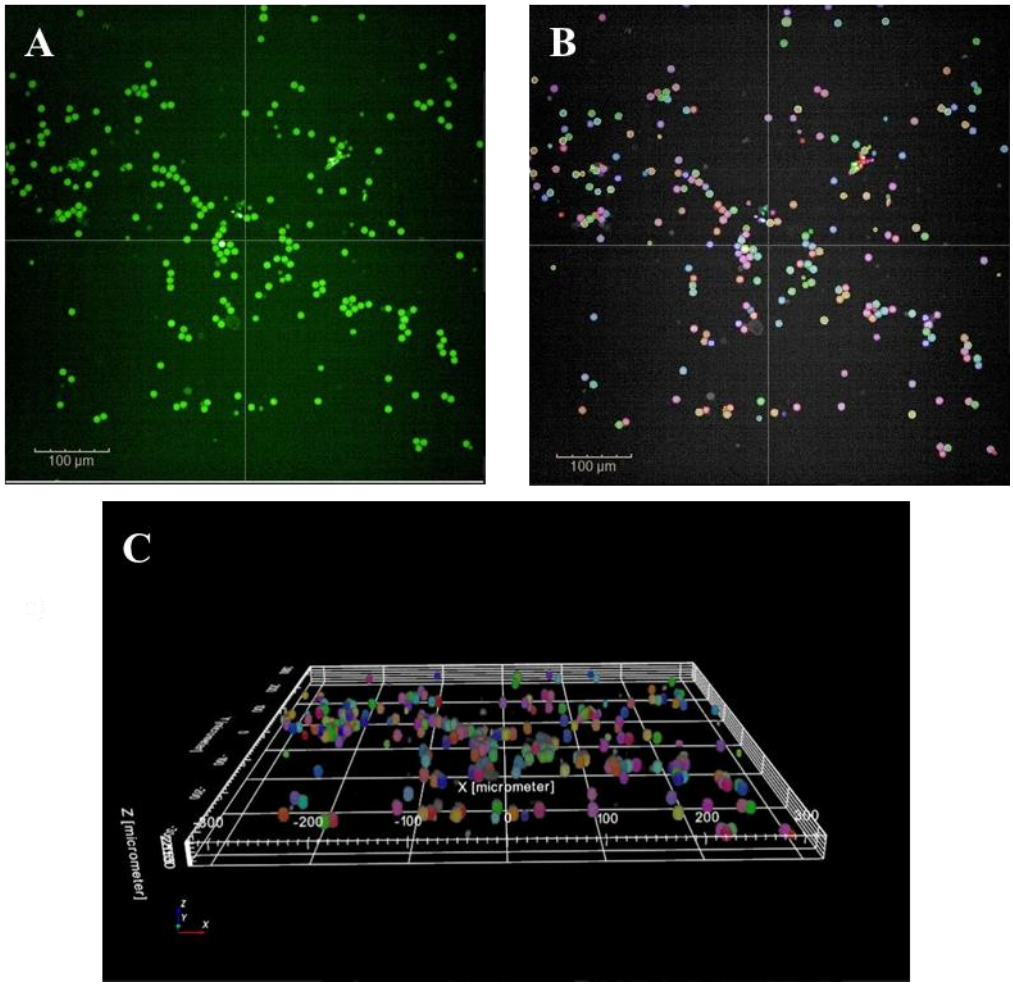

Figure 3.2: Image acquisition of microbeads using Opera Phenix. (A) Two-dimensional confocal image of microbeads was imaged using the 20x water objective (NA = 1) (Fluorescent channel = Alexa 488). (B) The Find Nuclei analysis tool from Harmony Software was used to create separate regions of interest (ROIs) for each microsphere within the field of view for volume calculations. (C) Z-stacks were processed and visualized in a three-dimensional setting with a z-height of 35 µm to ensure the entire height of the microparticle was included in the analysis.

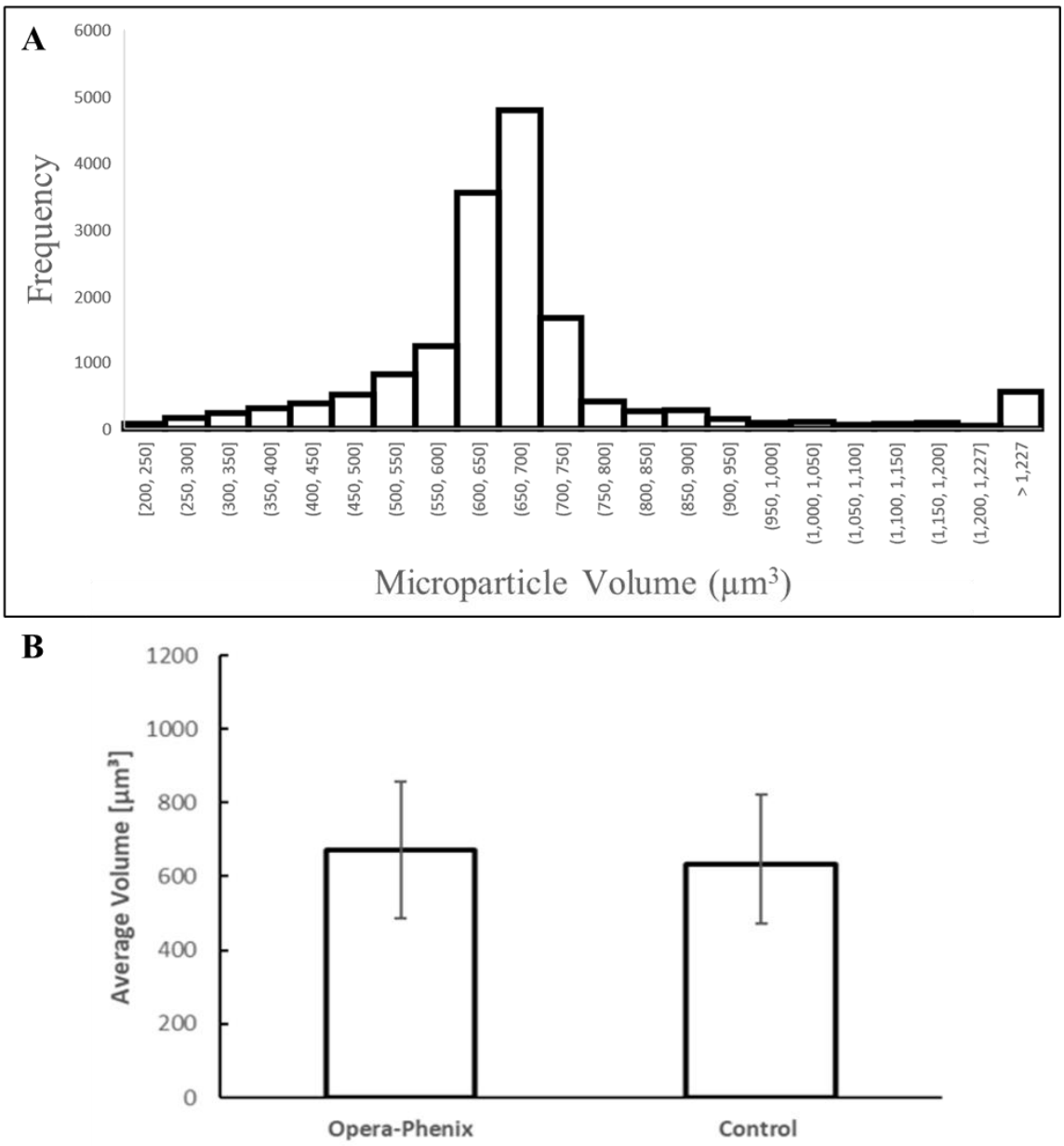

Figure 3.3: Volume measurement distribution and comparison of microbeads. (C) Distribution of microbeads showed a normal distribution across the three sample groups. The histogram contains a combined total of 15,893 microbead volume measurements across the three samples. (D) Volume measurement calculations comparing the known volume and deviation of the microbeads with the experimental calculation given from the Harmony Software. An average volume of $670.9 \pm 185.3 \mu m^3$ was measured via the Opera Phenix. Average volume calculations using the microbead parameters was found to be $631.9 \pm 174.1 \mu m^3$.

Due to the fact that the control group consisted of the calculated mean and standard deviation of the microbeads, a statistical comparison was not able to be performed between the two groups. However, the average volume measurement of the microbeads using the Opera Phenix was found to be within one standard deviation of the control measurements. Based on this, it can be assumed that the experimental volume measurements calculated via the Opera Phenix can be accepted for further experimental procedures.

3.2 Volume Analysis of 2D Adhered Cells

Volume measurements were calculated for human ovarian granulosa-like tumor cells (KGNs) that were adhered to the bottom of a culture treated glass bottom plate. This experimental outline provided an environment consistent with that seen within an *in vitro* two-dimensional cell culture. Optimal cell density for volume analysis was chosen by evaluating seeding densities of 50,000, 100,000, and 150,000 cells/well. A cell suspension of one-part Cell Tracker Green stained cells to ten-parts unstained cells (1:10) was seeded at 50K, 100K, and 150K densities in a CellView 96 well glass bottom plate and allowed to adhere via an overnight incubation period (T = 12 hours) at 37˚ C and 5% CO_2. Following the incubation period, the adhered cells were imaged, and single cell volume was analyzed using the Opera Phenix (Fig. 3.4). Cells seeded at a density of 50K cells/well resulted in the least overlapping of stained cells within the field of view. Conversely, cells seeded at a 150K density resulted in significant clumping and overlap of stained cells, making image analysis and separation of single cells difficult. Therefore, an optimal seeding density of 50K cells/well was used for the remainder of two-dimensional volume analysis.

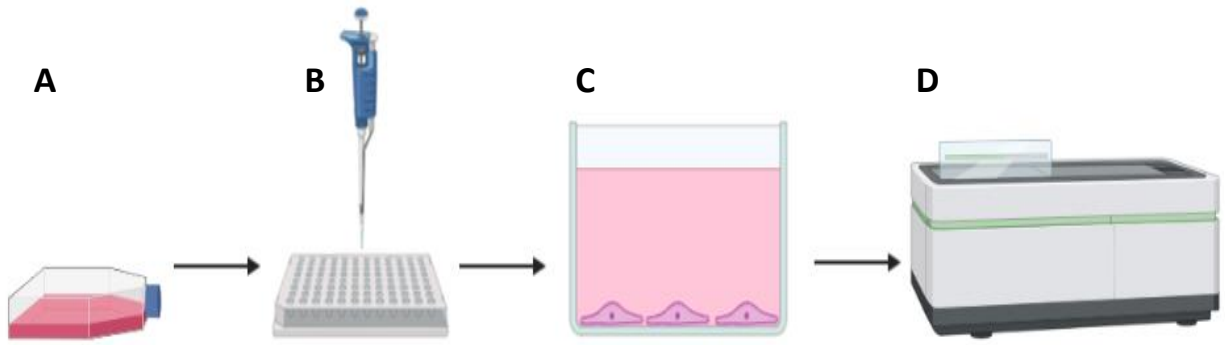

Figure 3.4: Experimental outline of adhered KGN cells in two-dimensional culture. (A) A cell solution of one-part CTG stained KGN cells to ten parts unstained KGN cells was created. (B) The KGN cell suspension was seeded into a CellView 96 well glass bottom plate at a seeding density of 50K cells/well. (C) KGN cells within the suspension were allowed to adhere to the bottom of the plate via an overnight incubation period (T = 12 h) prior to being imaged using the Opera Phenix (D).

Adhered KGN cells were imaged using cross sectional z-sections of 1µm for a total z-height of 50 µm. A 50 µm z-height allowed for imaging of the entirety of the adhered cells within the well. Adhered cells were imaged using the 20x water immersion objective (NA = 1) of the Opera Phenix. To determine the individual cell volume, image analysis was conducted using the Find Nuclei attachment from the Harmony software. The attachment separated individual adhered cells via the CTG staining channel into single regions of interest (ROIs). Volume analysis was conducted upon each of the ROIs for the total z-height of each cell (Fig. 3.5).

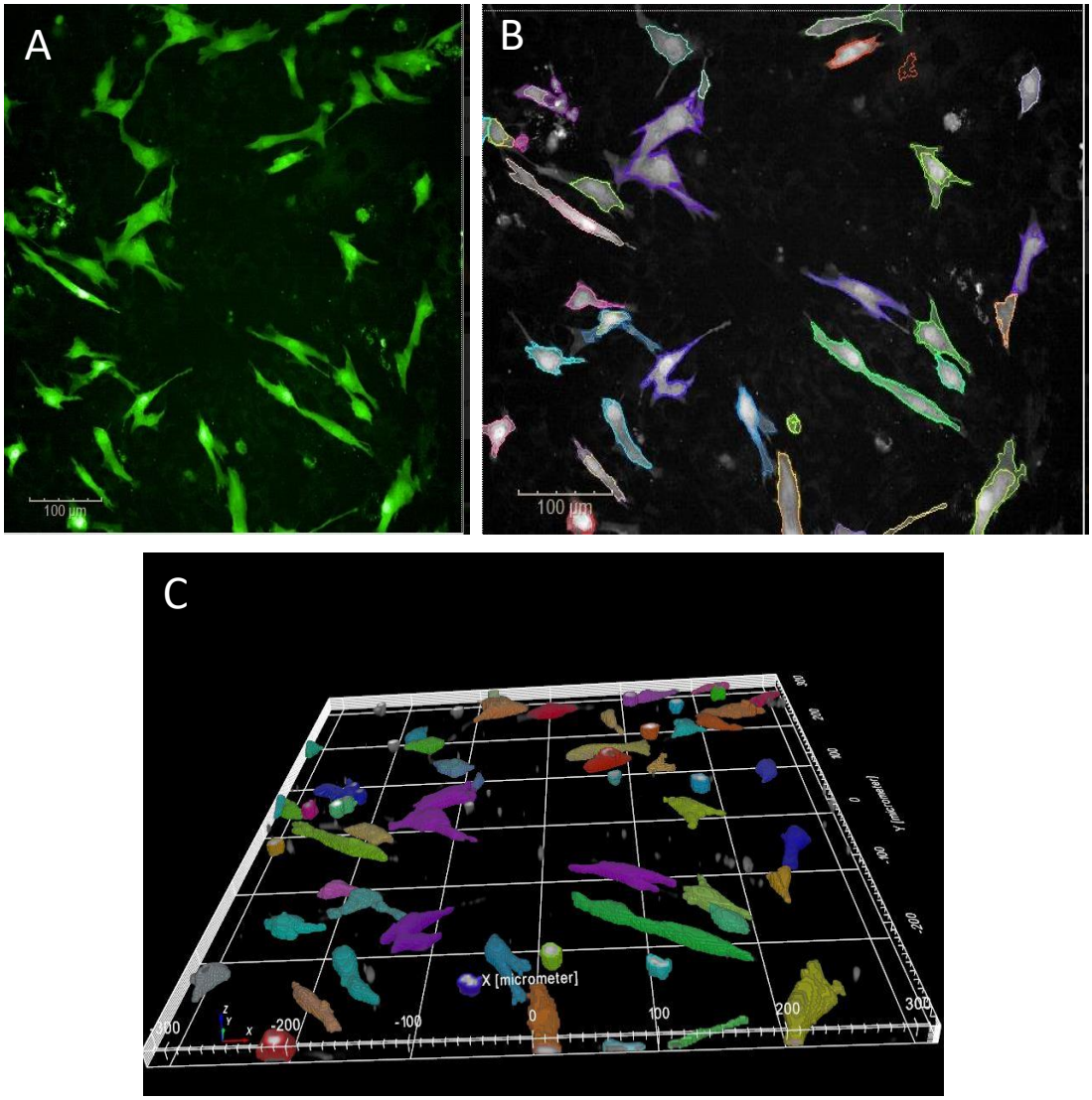

Figure 3.5: Confocal images of CTG stained KGN cells for adhered volume analysis (20x magnification). (A) Two-dimensional confocal image of 10% stained CTG KGN cell suspension seeded at 50K cells/well. (B) Two-dimensional Find Nuclei ROI construction separating individual cells for volume analysis. (C) Three-dimensional projection of CTG stained adhered KGN cells selected for volume analysis

Upon inspection of the automated ROIs formed during the analysis process, it was apparent that segmented cell regions of CTG were included in the volume analysis. These ROIs were not connotative of an individual cell, and if included in volume calculations would skew the measurements towards lower volume values (Fig. 3.6). Based on qualitative assessment of the

ROIs from the images, it was determined that volume measurements below the value of 1000 μm^3 would be excluded from the dataset and further volume analysis. On average, ROIs measuring beneath this value represented segmented sections of cells. Following image acquisition, volume measurements calculated below this value were filtered and excluded from the dataset.

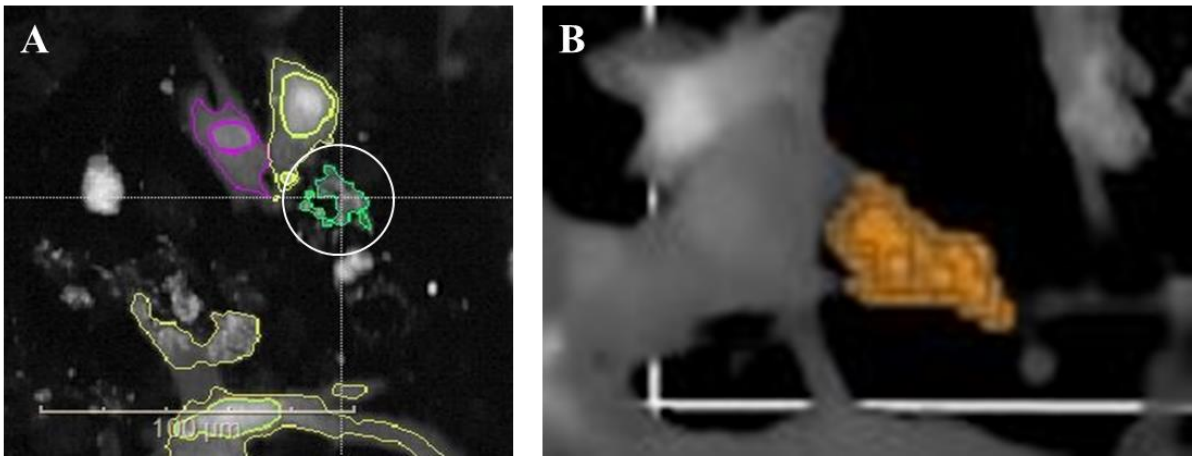

Figure 3.6: ROI analysis of segmented cell using Find Nuclei. (A) Two-dimensional image of automated ROI around a segment of CTG stained cell. (B) Three-dimensional projection of segmented cell ROI. Segmented cell ROIs were excluded from volume analysis.

In addition, single ROIs were also formed around multiple cells within close proximity to one another when using the Find Nuclei attachment (Fig 3.7). These ROIs were not connotative of an individual cell, and therefore would have skewed the measurements towards higher volume measurements. Therefore, volume measurements above 7000 μm^3 were excluded from datasets based on qualitative assessment of the analyzed images. On average, ROIs containing values above 7000 μm^3 consisted of multiple cells combined into one ROI. Therefore, following the

gathering of volume measurements, values above this upper threshold limit of 7000 μm^3 were filtered and removed from the resulting dataset and further volume analysis.

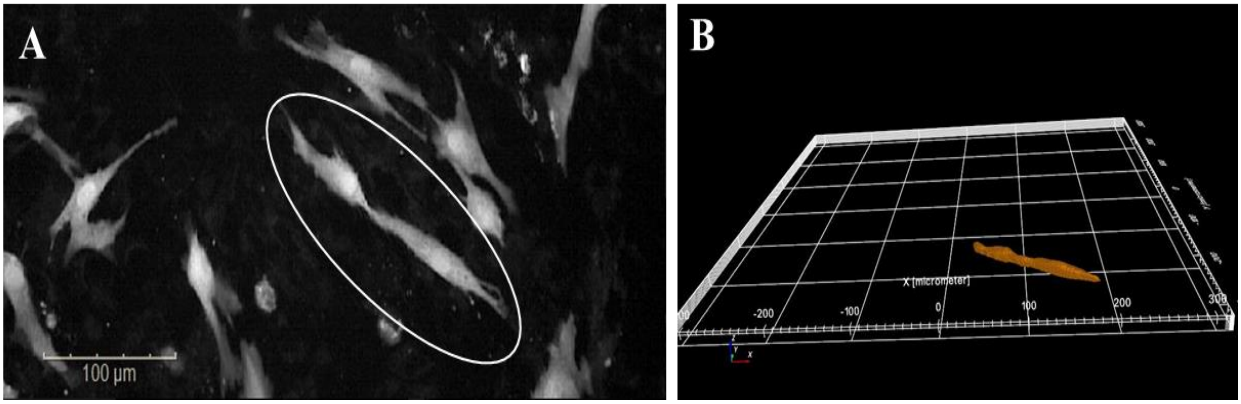

Figure 3.7: ROI analysis of merged cells. (A) Two-dimensional image of adhered KGN cells overlapping within the well during Opera Phenix imaging (20x magnification). (B) Three-dimensional projection of single ROI including the two cells.

Volume measurements of adhered KGN cells were acquired and filtered given the previous parameters (between the values of 1000 μm^3 and 7000 μm^3). Following the thresholding of the dataset, the average volume of adhered KGN cells was calculated. Within a two-dimensional cell culture environment, adhered KGN cells had an average cell volume of 3150 $\pm$ 1542 μm^3 (n=3) (Fig 3.8). This average was calculated via the combined volume data across the three biological samples. Given the skewed distribution of the dataset, the median value was also calculated from the three biological samples. The median measurement value across the adhered cell environment was found to be 2907 μm^3. Since the distribution of the volume measurements is skewed towards the higher values, a median value less than the calculated average was expected.

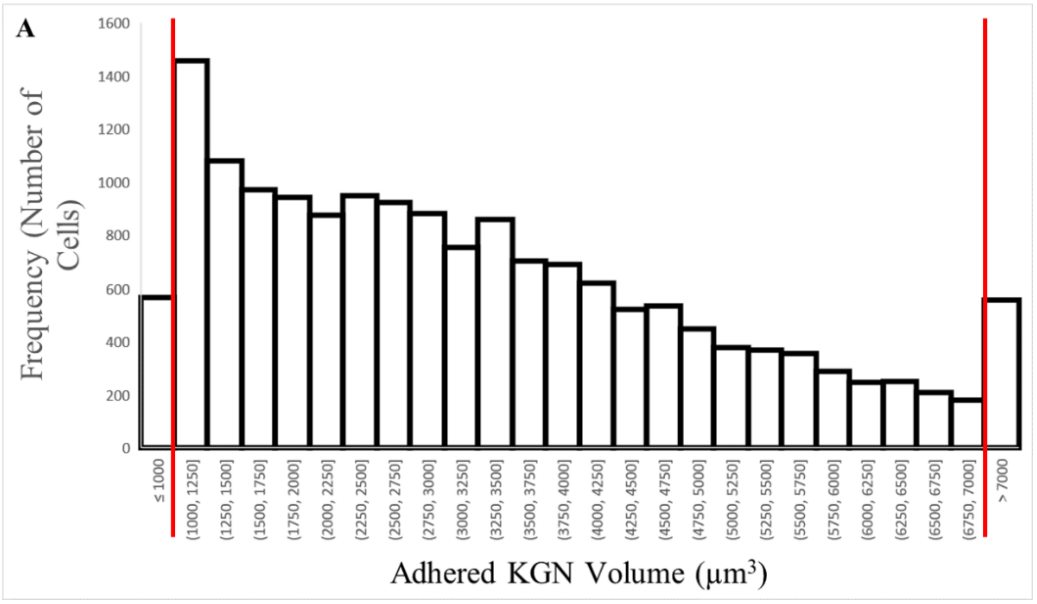

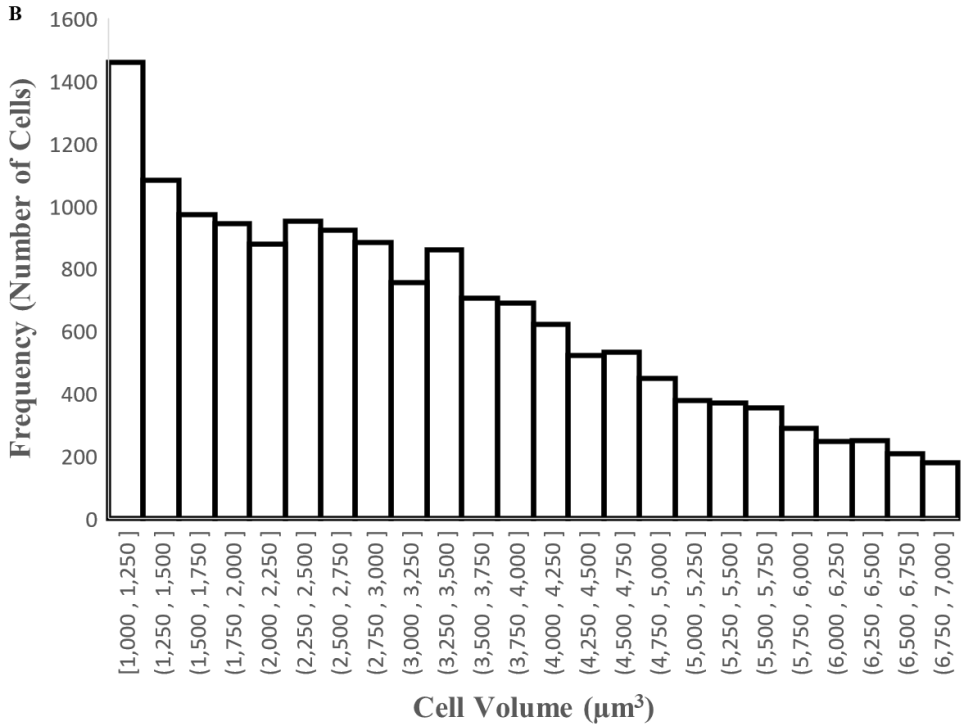

Figure 3.8: Single cell volume distribution of adhered KGN cells within a two-dimensional cell culture environment. (A) Unfiltered cell volume measurements including segmented and doublet cell analysis. Red lines show thresholding parameters of 1000 and 7000 µm^3. (B) Filtered cell volume measurements eliminating segmented and doublet cell ROI measurements. A combination of KGN volume measurements along three separate biological samples for a total value of 15,466 was plotted via a histogram. Given the volume measurements from the Opera Phenix, adhered KGN cells had an average cell volume of 3150 $\pm$ 1542 µm^3 (n=3). The median KGN cell volume measurement was found to be 2906 µm^3.

3.3 Volume Analysis of 2D Non-Adhered Cells

Volume measurements were than calculated for KGN cells that were not adhered within a two-dimensional cell culture environment. As seen previously, adhered KGN cells contain a morphology similar to that of a spindle. They are very elongated and do not maintain the spherical morphology that has been previously seen within three-dimensional microtissues (Fig 1.9). Therefore, an experimental outline was put forth to measure single cell volume of non-adhered KGN cells that contain a more spherical morphology, approximately consistent with that seen in single cells within microtissues.

A 10% CMFDA stained KGN cell suspension was established and seeded into a 96 well glass bottom plate lined with solidified 2% agarose. Solidified agarose is a non-adhesive material which blocks the cells ability to adhere to the surface via extracellular matrix (ECM) attachments. Therefore, KGN cells within this environment will maintain a spherical morphology more consistent to that previously described in microtissues.

The stained KGN cell solution was seeded within the agarose covered wells of a 96 well glass bottom plate and allowed to incubate overnight (T = 12 hours) prior to imaging with the Opera Phenix (Fig 3.9). The cells were imaged using z-sections of 1 µm for a total z-height of 50 µm. Average diameters of the nom-adhered cells were found to range between 10 and 20 µm, so this z-height would ensure image acquisition of the entire cell. The non-adhered cells were imaged using the 20x water immersion objective (N = 1) of the Opera Phenix. The Find Nuclei attachment was utilized to separate individual CTG stained cells within the field of view for subsequent volume analysis (Fig 3.8).

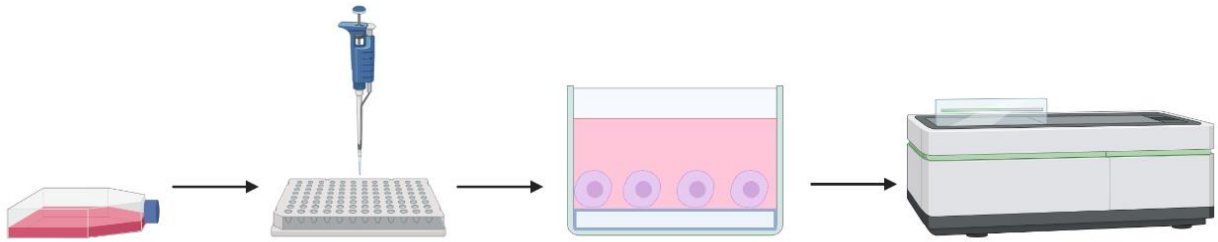

Figure 3.9: Experimental outline of non-adhered KGN cells in two-dimensional culture. (A) A cell solution of one-part CTG stained KGN cells to ten parts unstained KGN cells was created. (B) A layer of molten 2% agarose solution was pipetted into each well of the 96 well plate and allowed to cool and solidify. The KGN cell suspension was then seeded into a CellView 96 well glass bottom plate on top of the agarose at a seeding density of 50K cells/well. (C) KGN cells within the suspension were incubated overnight (T = 12 h) prior to being imaged using the Opera Phenix (D).

KGN cells seeded on the layer of agarose consistently had an increased spherical morphology when compared to that seen within the adhered condition. Similar to the adhered condition, it was necessary to filter the volume measurements using the parameters set forth previously to eliminate doublet cell measurements and segmented stained measurements. Qualitative assessment of the analyzed image suggested that the parameters of 1000 μm^3 and 7000 μm^3 were acceptable for filtering purposes of these datasets as well (Fig 3.10).

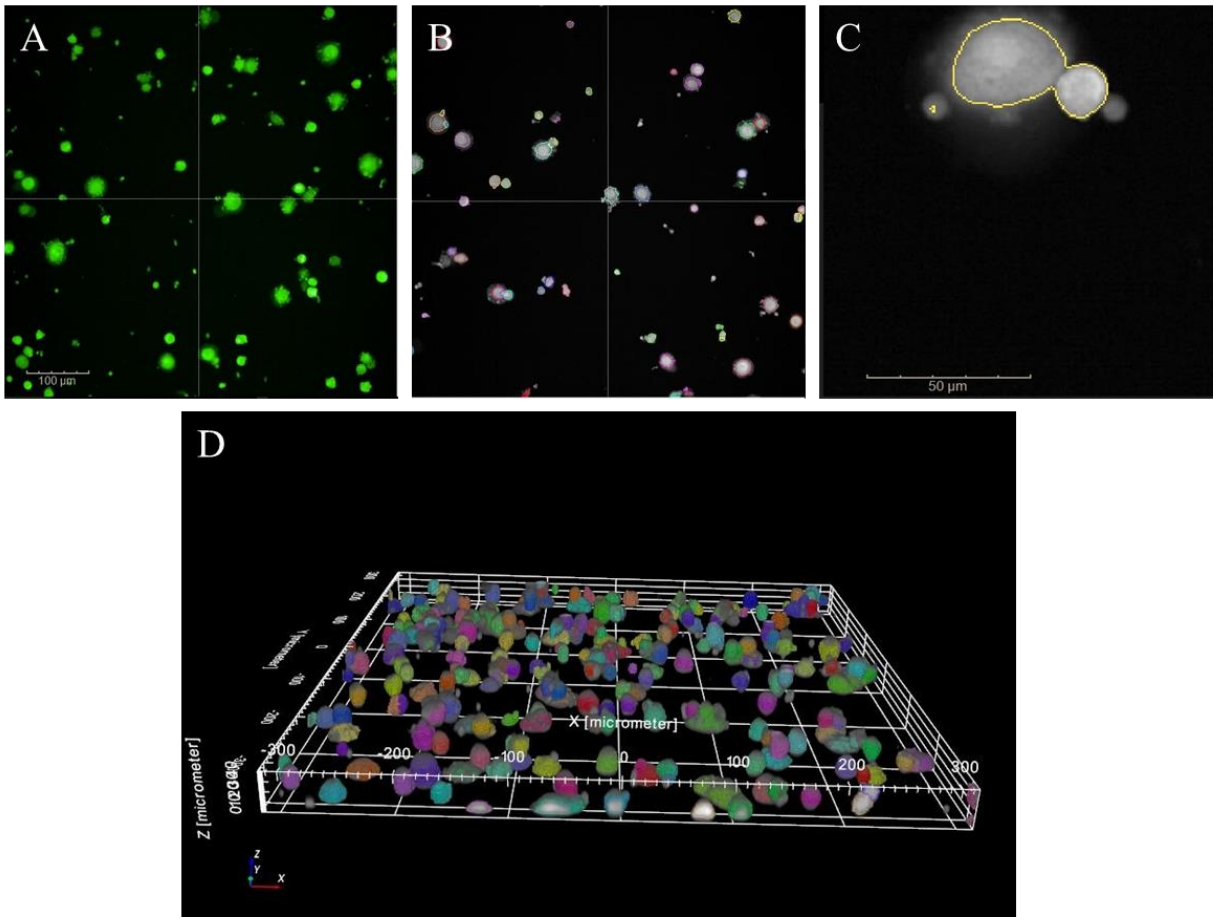

Figure 3.10: Confocal images of CTG stained KGN cells for non-adhered volume analysis (20x magnification). (A) Two-dimensional confocal image of 10% stained CTG KGN cell suspension seeded at 50K cells/well. (B) Two-dimensional Find Nuclei ROI construction separating individual cells for volume analysis. (C) Confocal field of view containing a doublet cell ROI measurement, as well as a segmented ROI construct. Average values from these ROI constructs were removed from the dataset for further volume analysis. (D) Three-dimensional projection of CTG stained non-adhered KGN cells selected for volume analysis. ROI analysis was completed for the entire z-height of the non-adhered cells within the system.

Volume measurements of KGN cells within a non-adhered environment were acquired and filtered using the previously stated parameters. Following the thresholding, the average volume of the dataset was calculated. KGN cells within a non-adhered environment containing a more spherical morphology, KGNs had an average cell volume of 2785 $\pm$ 1315 μm^3 (Fig 3.11). The average value was calculated using the combined dataset across three biological samples for

a total of 10,319 volume measurements. Given the skewed distribution of the graph, the median value was also calculated. The median volume measurement across the three samples was found to be 2522 μm^3. Given the distribution of the volume measurements was skewed to the right, it was expected that the median value of the volume measurements would be lower than the calculated average volume found within this condition.

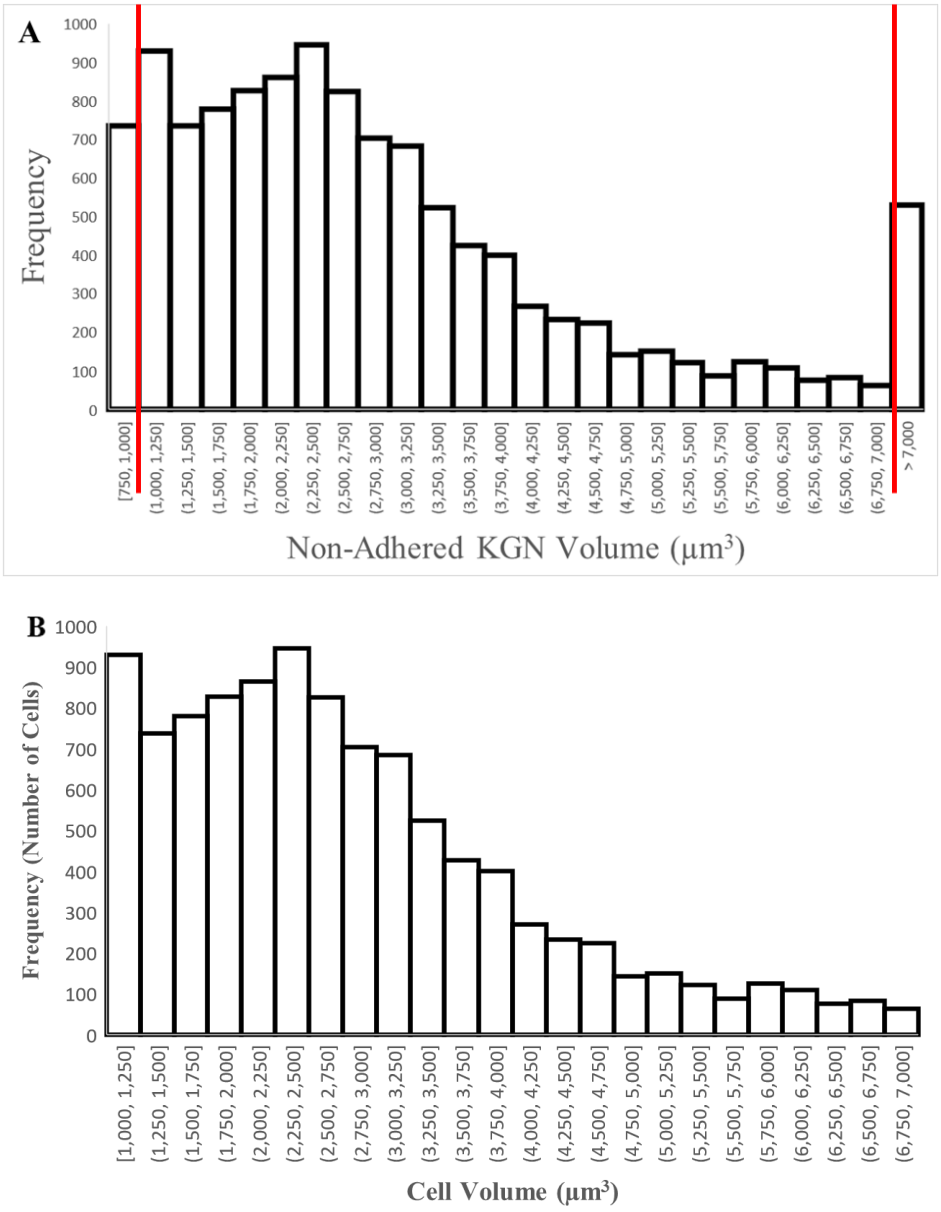

Figure 3.11: Single cell volume distribution of non-adhered KGN cells seeded on an agarose layer within a two-dimensional cell culture environment. (A) Unfiltered cell volume measurements including segmented and doublet cell analysis. Red lines show thresholding parameters of 1000 and 7000 µm^3. (B) Filtered cell volume measurements eliminating segmented and doublet cell ROI measurements. A combination of KGN volume measurements along three separate biological samples for a total value of 10,319 measurements was plotted via a histogram. Given the volume measurements from the Opera Phenix, non-adhered KGN cells had an average cell volume of 2785 $\pm$ 1315 µm^3 (n=3). Given the skewed distribution of the graph, the median KGN cell volume measurement was calculated as well and found to be 2522 µm^3.

Chapter 4

Analysis of Cell Volume in Three-Dimensional Culture

4.1 Single Cell Volume Analysis within Microtissues

The calculation of single cell volume within the constructs of a three-dimensional microtissue has yet to be fully measured. Previous experiments and models have suggested that single cell volume within microtissues appear to decrease when extrapolated from total microtissue volume. To determine the change of single cell volume within a three-dimensional culture environment, KGN cells were seeded at 5,000 cells per spheroid in micro-molded agarose gels. The cell suspension consisted of a 1:10 part ratio of cells stained with CTG to unstained cells. Theoretically, this would result in 500 cells per spheroid being stained and capable of being imaged using the Opera Phenix. The spheroids were allowed to self-assemble for 30 min prior to being incubated overnight (T = 12 hrs). The overnight incubation ensured that the spheroids would maintain structural integrity when being transferred between plates. Prior to imaging, spheroids were removed from the agarose molds and placed in individual wells within a CellView glass bottom 96 well plate.

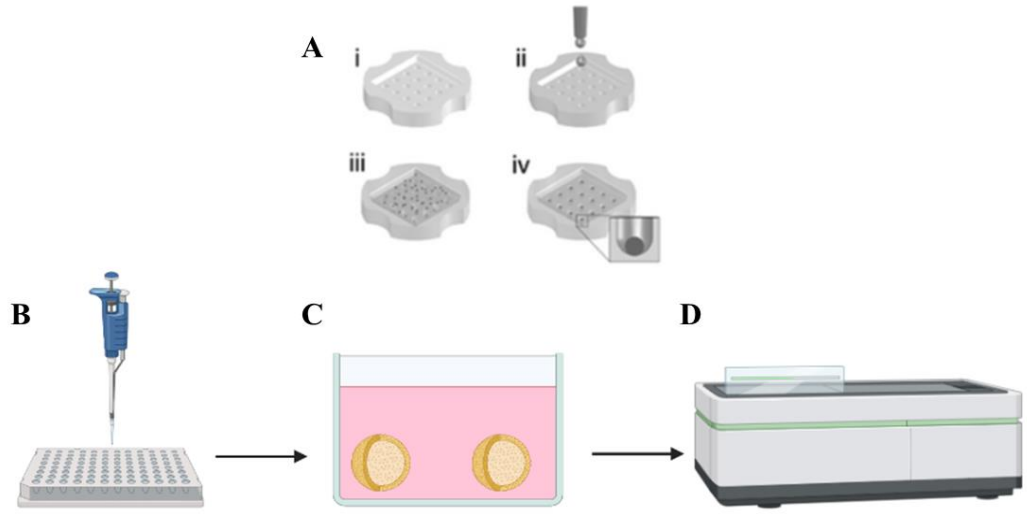

Figure 4.1: Experimental outline of 10% CTG stained KGN spheroids in three-dimensional culture. (A) A 10% CTG stained KGN cell solution was seeded at 5000 cells/spheroid within micro-molded agarose gels and allowed to self-assemble (B) Following formation of the KGN spheroids, the microtissues were transferred from the agarose gels to individual wells of a 96 well plate using a P-1000 pipette. (C) KGN spheroids within the individual wells were incubated overnight (T = 12 h) prior to being imaged using the Opera Phenix (D).

Individual spheroids were then imaged using the Opera Phenix to analyze single cell volume of individual cells (Fig 4.1). Images were acquired using z-sections of 1 µm across a total z-height of 250 µm. The average height of spheroids was found to be approximately 150 µm, so the image acquisition up to 250 µm would ensure imaging of the entire height of the spheroid. The 10% stained cell suspension allowed for imaging of single cells at different positions within the spheroid structure (Fig 4.2).

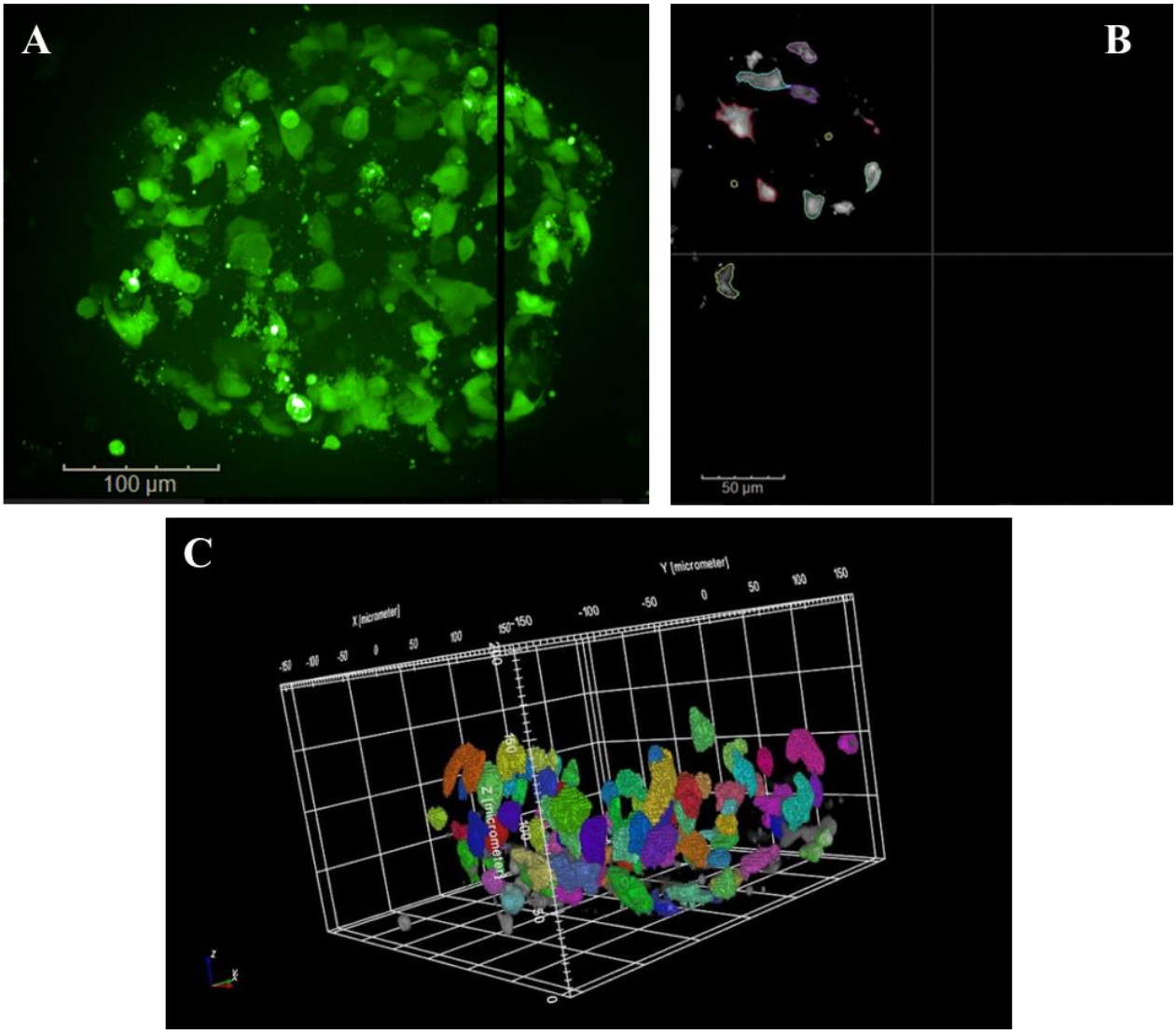

Figure 4.2: Opera Phenix images of CTG stained KGN cell spheroids (40x magnification). (A) Two-dimensional confocal image of 10% stained CTG KGN cell spheroid seeded at 5,000 cells/spheroid. (B) Two-dimensional Find Nuclei ROI construction separating individual cells for volume analysis within the spheroid. (C) Three-dimensional projection of individual CTG stained KGN cells within the spheroid microtissue. ROI analysis for volume measurements was observed throughout the entirety of the height of individual cells within the spheroid.

One limitation that was presented when acquiring single cell volume within the microtissue construct was distinguishing between ROI constructs formed around doublet cells. When analyzing in two-dimensional culture environments, it was clearly distinguishable between multiple cells within close proximity that were measured as a single cell using the ROI

attachment. This technique was not applicable when imaging in three-dimensional culture, and therefore spheroids were additionally stained with a Hoechst stain solution. Cells were stained with a CTG and Hoechst stain solution for 30 minutes prior to microtissue seeding. A cell suspension consisting of a 1:10 part ratio of CTG/Hoechst stained KGN cells to unstained KGN cells were seeded at 5000 cells per spheroid in micro-molded agarose gels. The spheroids were incubated for 30 min to allow for self-assembly. The spheroids were then incubated overnight (T=12 hrs) to allow for transfer of the microtissues from the agarose mold to individual wells within a 96 well CellView plate.

Nuclear staining of cells within the spheroid using the Hoechst stain solution allowed for visualization of individual nuclei within the stained cells in the microtissue (Fig 4.3). The staining procedure was successful in determining volume measurements consisting of multiple cells within close proximity to one another within the spheroid. Analysis of average volume measurements of doublet cells using the Harmony software concluded that the previously accepted threshold of 7000 μm^3 was acceptable for filtering the three-dimensional volume dataset. Consistent with that seen in two-dimensional cultures, volume measurements greater than this threshold represented ROIs formed around multiple cells within close proximity to one another.

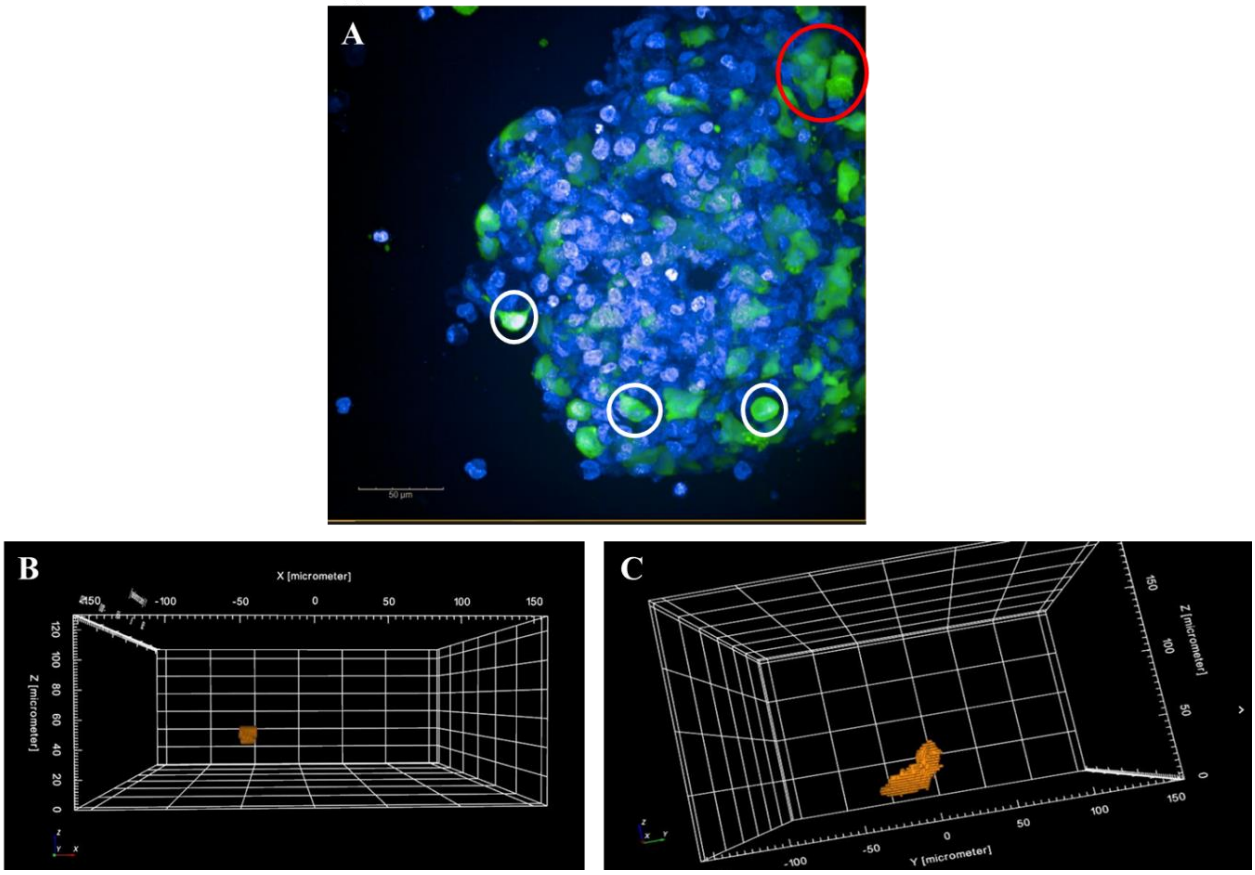

Figure 4.3: Analysis of ROI formation around multiple cells within the spheroid. KGN cells were stained with both CTG and Hoechst prior to formation of 5000 cell/spheroid microtissues. A 1:10 part suspension of CTG/Hoechst-stained cells to unstained cells respectively was used for seeding purposes. (A) The Hoechst staining allowed for visualization of nuclei of single cells within the CTG stained KGNs. White circles represent single cells stained with CTG capable of being used for volume analysis. The red circle represents regions of the spheroid where multiple cells are within close proximity to one another, where single ROIs are formed around multiple cells. (B) Three-dimensional confocal rendering of a single cell ROI formed within the microtissue construct. (C) Three-dimensional confocal rendering of single ROI formed around multiple cells within the red circular region not applicable to single cell volume analysis.

Volume measurements of single cells within a three-dimensional spheroid were acquired and filtered against the parameters previously given and accepted via the nuclear staining (range of volume measurements between 1000 μm^3 and 7000 μm^3). Within a three-dimensional microtissue environment, individual KGN cells had an average volume measurement of 2442 $\pm$

1307 μm^3 (Fig 4.4). As seen with both two-dimensional conditions, the distribution of volume measurements across the three samples was skewed to the right. The median volume across the samples was found to be 2014 μm^3. The average volume measurements of individual cells was calculated through the combined dataset of the three biological samples, consisting of 5,239 total samples.

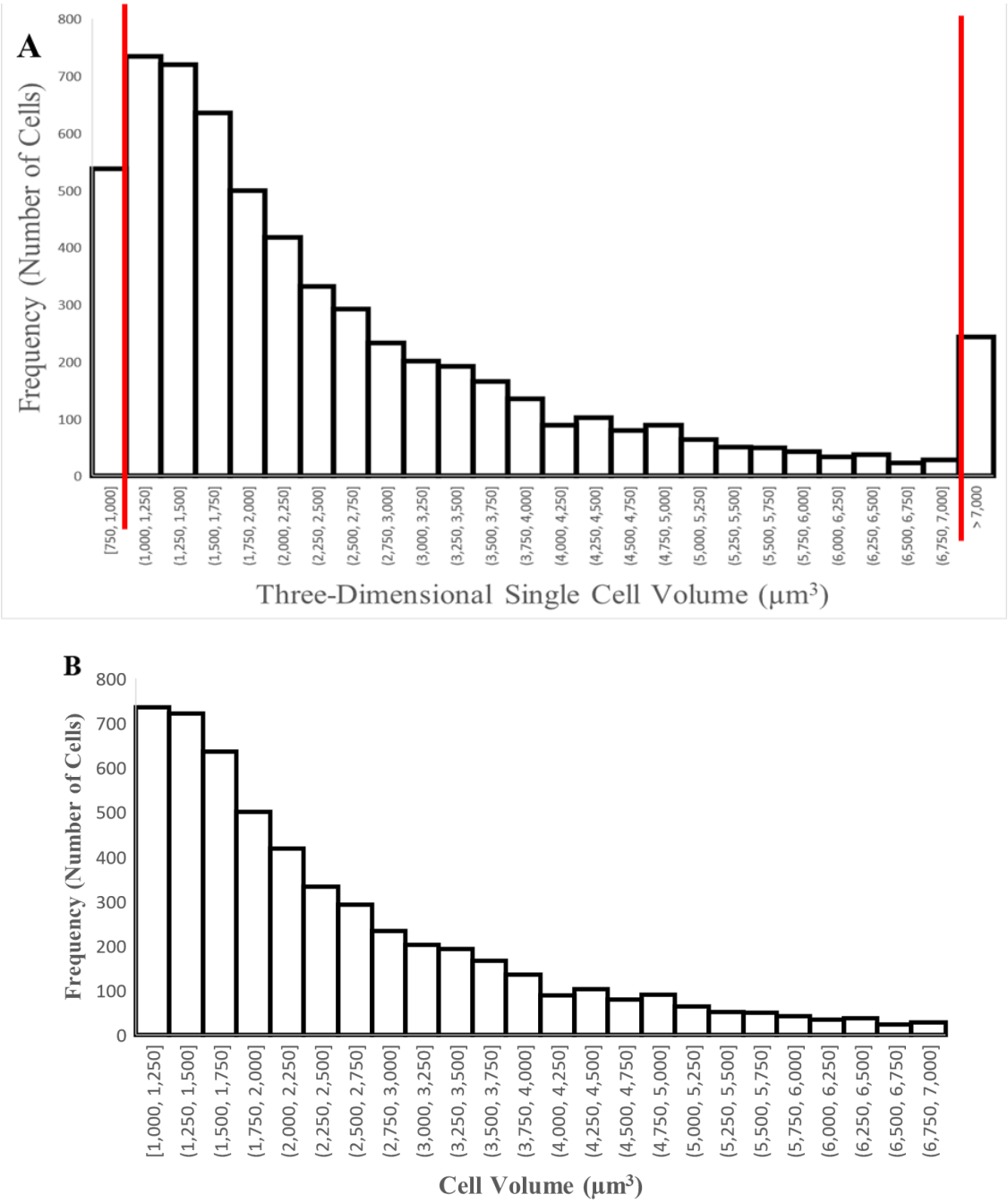

Figure 4.4: Single cell volume distribution of KGN cells within a three-dimensional microtissue environment. (A) Unfiltered cell volume measurements including segmented and doublet cell analysis. Red lines show thresholding parameters of 1000 and 7000 µm^3 which were confirmed via Hoechst nuclear staining. (B) Filtered cell volume measurements eliminating segmented and doublet cell ROI measurements. A combination of KGN volume measurements along three separate biological samples for a total value of 5,239 measurements was plotted via a histogram. Given the volume measurements from the Opera Phenix, single KGN cells within a spheroid had an average cell volume of 2442 $\pm$ 1307 µm^3 (n=3). Given the skewed distribution of the graph, the median KGN cell volume measurement was calculated as well and found to be 2014 µm^3.

Comparison of the volume distributions across the three environmental conditions suggests that single cell volume decreases within three-dimensional culture conditions when compared to two-dimensional conditions (Fig 4.5). The average volume measurement of single cells decreased between the adhered cell environment, non-adhered cell environment, and microtissue environment. This was shown with the average volume measurements across the three conditions of 3150, 2785, and 2442 μm^3. Comparison of single sample means between the three conditions via a One-way ANOVA and Tukey multiple comparison test suggested that there was a difference in cell volume between each of the three conditional groupings ($p < .05$) (Fig 4.6).

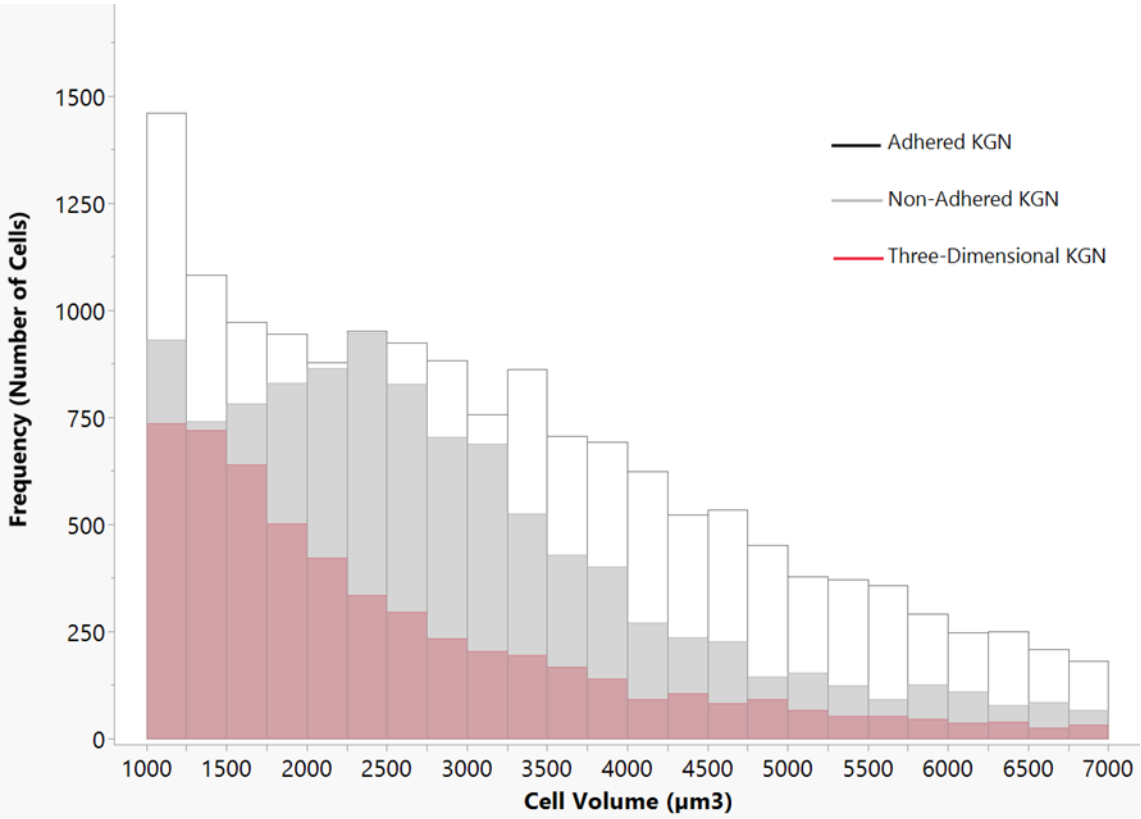

Figure 4.5: Comparison of single cell volume distribution between 2D and 3D culture conditions. Superimposed histogram displaying volume measurement distribution between 2D adhered, 2D non-adhered, and 3D microtissue single KGN cells. The distribution suggests that single KGN cells within a three-dimensional spheroid environment have lower volume measurements when compared to two-dimensional culture conditions.

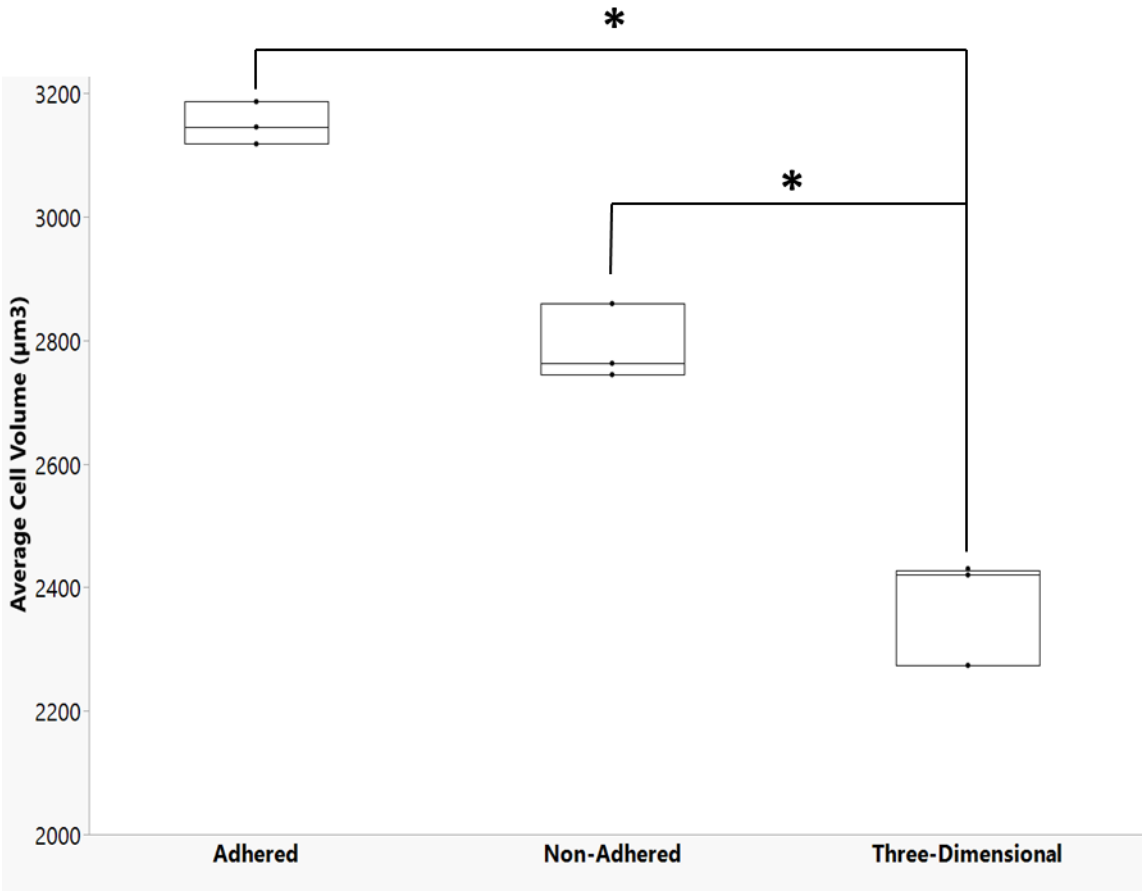

Figure 4.6: Statistical analysis between adhered, non-adhered, and three-dimensional single cell volume. Average volume measurements from individual biological samples between the three conditions were compared via a Oneway ANOVA and Tukey multiple comparison test. Normality of the data was tested using a Shapiro-Wilk Goodness-of-fit test ($p > .05$). The data suggests a variation in single cell volume size between each conditional group (* denotes $p < .05$).

To quantify the effect cell position within the spheroid had on overall single cell volume, KGN volume measurements were acquired and compared between cells on the outer surface of the spheroid and cells within the interior region of the spheroid. 21 single cells were acquired and quantified within each three-dimensional sample group (n=3) based on the following inclusion parameters. KGN cells located on the outer surface of the spheroid were chosen for inclusion within the surface region group. Cells acquired from the inner region of the spheroid had to be located 20 µm away from the outer surface of the spheroid (Figure 4.7). Cells located

within the inner region of the spheroid showed a significant decrease in volume when compared to those located on the outer surface using a two-tailed, unpaired t-test with Welch's correction ($p = .0206$). Overall, the volume measurements within the surface region of the spheroid were significantly higher than those seen within the inner regions of the spheroid (Fig 4.8).

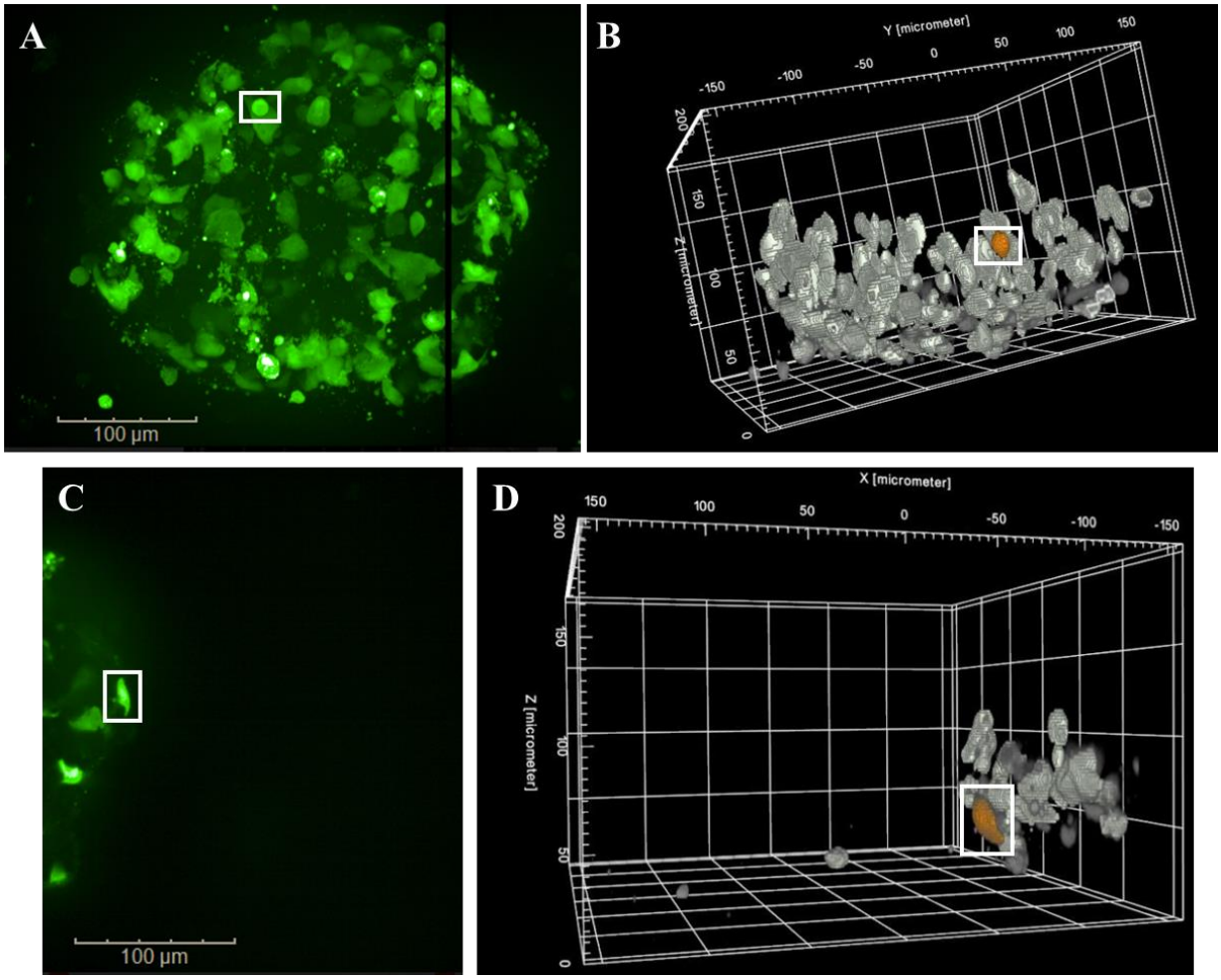

Figure 4.7: Assessment of KGN cells located within the surface and inner regions of the spheroid. (A) 10% CTG stained KGN spheroid seeded at 5,000 cells was imaged using 20x magnification with the Opera Phenix. Boxed cell denotes an applicable cell for volume measurement within an interior position within the spheroid (greater than 20 µm from the spheroid surface). (B) Three-dimensional rendering of the interior positioned cell within the spheroid. (C) Boxed cell indicates a cell assessed as positioned on the surface region of the spheroid. (D) Three-dimensional rendering of the surface positioned cell utilized for cell volume measurements.

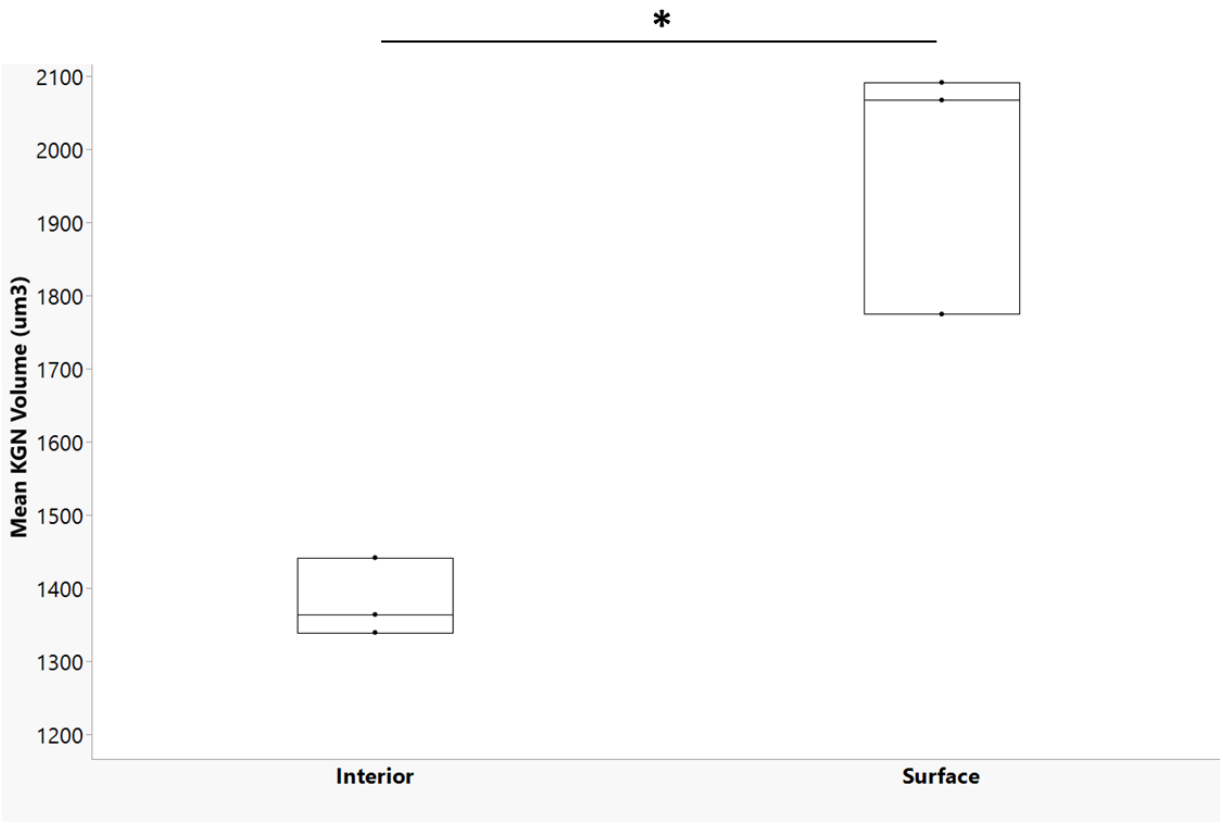

Figure 4.8: Statistical analysis between interior and surface positioned cells within a spheroid. 21 KGN cell volume measurements were randomly selected and analyzed within each of the 3 sample groups and compared via two-tailed, unpaired t-test with Welch's correction. Normality of the data was measured using a Shapiro-Wilk Goodness-of-fit test ($p > .05$). The data suggests that the average volume between positional region of the spheroid is significantly different. Cells located on the surface of the spheroid have significantly greater cell volume than those found within the interior of the tissue (* denotes $p < .05$).

Chapter 5

Discussion and Future Directions

The data presented within this thesis established a technique to compare cell volume between two-dimensional and three-dimensional culture conditions. The three experimental outlines performed were chosen to portray adhered cells within two-dimensional culture, non-adhered cells within two-dimensional culture, and cells within a three-dimensional microtissue culture.

The Opera Phenix High Content Screening System was found to provide an acceptable measuring technique for single cell volume across the varying conditions. A proof-of-concept for volume analysis was conducted using fluorescent microbeads of a known volume. The volume measurements of Polysciences violet microbeads were acquired via the Opera Phenix and compared to volume measurements found using the control specifications of the microbeads. The volume measurements of the microbeads using the Opera Phenix were found to follow a normal distribution trend across the three samples. The presence of a normal distribution allowed for experimental calculations to be compared to the control values using a mean and standard deviation comparison. The mean volume measurement of the microbeads found using the Opera Phenix was found to fall within one standard deviation of the control volume mean. Therefore, the data suggested that the Opera Phenix experimental system was an appropriate system for measuring cell volume within a three-dimensional analysis. One limitation presented within this analysis was the inability to run statistical analysis between the two means. Due to the fact that the control volume measurements were found using the average diameter range specifications

given from Polysciences, and not an appropriate sample set, the experimental dataset could not be analyzed against the control calculations via statistical analysis testing.

Quantification of single cell volume of KGNs within a two-dimensional adhered culture condition was evaluated. Using the Opera Phenix, CTG stained KGN cells which were allowed to adhere to a glass bottom 96 well plate was imaged and analyzed for volume measurements. Cells within this environment were seen to contain a flattened, spindle like morphology (Fig 3.5). This was due to the presence of extracellular matrix interactions with the glass bottomed well. ECM attachment to the glass bottom resulted in the spreading of the cell across a greater area, resulting in this morphology. The distribution of volume measurements gathered within this environment differed than that seen within the fluorescent microbeads. While the microbeads contained a normal distribution across volume measurements, the adhered cells volume measurements included a positive skew. The distribution of measurements was skewed towards higher values due to the increased variability when compared to the microbeads. For this reason, both the average volume measurements and median volume measurement was presented for this condition.

Having quantified single cell volume of KGN cells within an adhered morphology, non-adhered cell volume was quantified. KGN volume of cells seeded on a non-adherent agarose surface were found to contain a slightly lower average volume when compared to adhered cells. Agarose was used to promote a non-adhered cell environment due to its physical properties minimizing cell attachment via the extracellular matrix. Agarose gel lacks the cell binding motifs necessary for ECM interactions with the substance (Vries (2020)). Therefore, cells seeded on agarose promote a more spherical morphology when compared to the spindle morphology seen within adhered KGN cells. The elimination of ECM interaction with the agarose limits cell

adhesion and flattening, resulting in this spherical morphology. The qualitative analysis of individual non-adhered cells within this condition portrayed the addition of merged cell ROIs and segmented stained regions that were imaged and viewed as a single ROI. The Find Nuclei attachment in the Harmony software is fully automated and does not allow for manual thresholding of formed ROIs within the acquired images. The merged and segmented ROIs formed were easily quantified by visual inspection of the acquired three-dimensional images. Therefore, after analysis of these groupings of measurements, it was determined that the parameters of 7000 μm^3 and 1000 μm^3 set forth via the adhered cell measurements were acceptable for filtering non-adhered datasets as well. As seen with the volume distribution of adhered KGN cells, non-adhered KGN volume distribution also followed a skewed distribution (Fig 3.8). The volume measurements contained a positive skewed trend, with a tail visible towards higher volume measurements, consistent with that seen in the adhered cell condition. For this purpose, both the average volume measurement and median volume measurement were presented. Both the average and median volume measurements of the non-adhered KGN cells suggested lower single cell volume measurements than those seen within the adhered cell condition.

Quantification of single cell volume within a three-dimensional spheroid construct was then assessed and compared to the two-dimensional culture conditions. This process involved the formation of spheroidal microtissues with a 10% CTG stained cell solution. The use of a 10% stained cell suspension allowed for the ability to visualize and distinguish individual cells within the greater microtissue construct. The process involved transferring spheroids from the agarose micro-mold to wells within a 96 well plate. This transferring step could have affected the overall shape and morphology of the spheroid shape.

Initial imaging of the 10% stained spheroid presented a limitation within the volume measurements acquired via the ROI analysis. Unlike in the two-dimensional culture conditions, it was difficult to distinguish individual ROI measurements of multiple cells and segments of cells within the microtissue. Therefore, it was necessary to stain individual cell nuclei with Hoechst in addition with the CTG staining. This allowed for the assessment of ROIs formed around groups of cells containing multiple nuclei within close proximity to one another within the tissue. Therefore, accurate filtering parameters for the dataset could be assessed for volume measurements acquired within the three-dimensional culture. Interestingly, when spheroids stained with both Hoechst and CTG were imaged using the Opera Phenix, there appeared to be an increased number of KGNs stained with Hoechst than CTG. The same 10% stained cell suspension was utilized for this experiment; therefore, the same number of cells should have been labelled with CTG and Hoechst. However, the stained spheroids were incubated overnight prior to image acquisition. During this overnight incubation period, the Hoechst stain could have permeabilized through the stained cells membranes and inadvertently stained cells within the surrounding area of the spheroid. While Hoechst stain remains permeable following cell staining, this is not the case with CTG. Once the CTG stains the cell, it becomes impermeable to other cells within surrounding environment, eliminating the possibility of leaching to other cells.

As seen within the two-dimensional conditions, the distribution of single cell volume within a spheroid also contained a positive skew. Therefore, the average and median volume measurements were presented for this condition. To evaluate the cell volume between the three environmental conditions, a Oneway ANOVA with Tukey multiple comparison test was performed using an alpha level of 95%. Based on the trend seen within the superimposed histogram of the three conditions (Fig 4.5), the data suggested that the single cell volume within

the spheroid was lower than that seen within the two-dimensional conditions. The ANOVA and Tukey multiple comparison test further suggested that average cell volume decreases between the three environments. Adhered cells were found to have the highest average cell volume, followed by non-adhered cells and single cells within a microtissue. This was consistent with the original hypothesis that cells within a microtissue environment had lower volumes when compared to two-dimensional culture. However, a notable limitation present within this study is the inclusion of confounding variables such as passage number and experimental timing. The adhered, non-adhered, and three-dimensional cell experiments were not completed at the same time. The samples of adhered cells were initially analyzed, followed by the non-adhered and three-dimensional conditions. Therefore, cells across the three conditions contained varying passage number and subsequent cell age. However, all cells were analyzed within passage numbers of 11 to 14, and therefore the potential of cell volume decrease due to senescence can be eliminated.

Evaluation of cell volume based on positional location within the spheroid was conducted across the three 3D culture biological samples. KGN cells located on the surface of the spheroid and within the interior of the spheroid were analyzed and compared. KGN cells were randomly chosen given the inclusion parameters previously set forth for each position group and analyzed via a two-tailed, unpaired t-test with Welch's correction. Cells located on the outer surface of the spheroids had significantly greater volume measurements when compared to cells within the interior of the tissue. This is consistent with previous models suggested by Shenoy et al. (Fig 1.9). Cells located within the inner regions of the spheroids tend to have increased solid stresses enacted upon them, causing a subsequent decrease in cell volume (Shenoy (2020)). Further experimentation could be conducted to quantify the forces presented within the interior regions

of the spheroid and quantify the magnitude change these forces have when compared to the surface regions of the spheroid. It is also possible that the mechanosensitive channels of the cells within the interior region of the spheroid are closed due to the hypothesized increased stress levels. This would limit the transport of ions into and out of the cellular environment, seen with the regulatory volume channels, and affect the cell's ability to maintain a constant cell volume. To determine whether the mechano-sensitive ions are closed, or whether there is a dysfunction in the regulatory channels, potassium and chloride concentrations could be measured in the extracellular spheroidal media over time. Previous research showed that increasing levels of potassium and chloride within the extracellular environment was associated with apoptotic volume decrease (Fig 1.3).

In addition, varying surface morphology between cells on the surface and cells within the interior of the spheroid could also suggest a reason for varying volume measurements. As seen through the cell volume measurements between adhered and non-adhered cells, adhered cells tended to have slightly higher volume measurements of the two conditions. These adhered cells contain a morphology more consistent with that seen from cells on the surface of spheroids. As seen in Figure 4.7C, cells on the surface have a flatter, more spindle like morphology consistent with that seen in adhered culture (Fig 3.5). In comparison, cells within the interior of the spheroid tend to have a more spherical morphology similar to that seen within non-adhered cells (Fig 4.7).

Overall, results suggested that a measurement of single cell volume within a microtissue can be obtained using the Opera Phenix High Content Screening System. The experimental outline set forth allowed for comparison of cell volume within varying culture conditions, as well as between varying locations within a three-dimensional microtissue. This technique can be used

in the future to further study the effect of single cell volume within a microtissue construct. Future directions for this work would be to perform single cell volume analysis on microtissues of varying shapes. Previous data has suggested that total volume within tissue rings decrease over time (Fig 1.8). The outline set forth in this thesis could be adapted and utilized on varying microtissue shapes and sizes to validate that the result is consistent across three-dimensional culture. The utilization of varying cell types would also further validate the results found within this thesis. One limitation presented within this outline was the inclusion of only one cell type for experimental purposes (KGN cells). Primary human umbilical vein endothelial cell (HUVEC) lines or human hepatocytes (HepG2) could be tested to validate that this phenomena is consistent across varying cells. In addition, volume measurements could be acquired over varying time points to determine whether there is a subsequent decrease in volume measurement at later time points. Previous work has suggested that microtissue cell volume decreases over time (Fig 1.8). A next step would be to test single cell volume at varying time points after microtissue formation to determine whether this decrease in tissue volume is due to further decrease in volume of the cell bodies or decreasing position between individual cells. This technique also allows for future work to determine whether the volume of cell bodies within a microtissue varies based on changes in osmolarity, microtissues could be cultured in media with varying hyperosmotic factors. Previous research has suggested that overall microtissue volume changes with respect to varying osmotic environments (Fig 1.6). This would allow for observation as to whether this varying microtissue volume is a result of varying single cell volume within the microtissue.

Chapter 6

Summary and Conclusion

There has been an increasing desire within the Bioengineering field to develop *in vitro* modeling techniques mimicking *in vivo* environments for tissue engineering and drug development purposes. Three-dimensional microtissues have the ability to be used as building blocks for larger 3D constructs, as well as being an appropriate method for drug testing and development prior to *in vivo* trials. Therefore, there is a need to understand the biological structures and mechanisms of said microtissues to further the advancement of this field. Theoretical decreases in total volume have been previously recorded within three-dimensional microtissues. It was unclear what was the overlaying cause of this decrease, and whether it was a decrease within single cell volume within the construct specifically. The Opera Phenix High Content Screening System is a confocal technique utilized for three-dimensional image acquisition of biological samples. The work of this thesis aimed to develop an imaging technique capable of measuring single cell volume within a three-dimensional culture environment. Results suggested that single cell volume within a spheroid microtissue was decreased when compared to cells within two-dimensional adhered and non-adhered environments. Furthermore, varying cell position within the microtissue was seen to associate with differences in cell volume measurements. Cells positioned within the interior positions of the spheroids were lower than those seen on the surface. Ultimately, the techniques presented within this thesis to evaluate single cell volume within microtissues could be used to further evaluate factors which may affect

cell volume within microtissues and the biological effect they present on the overall microtissue structure.

Bibliography

Alvarez-Román, R., Naik, A., Kalia, Y. N., Fessi, H., & Guy, R. H. (2004, September 1). Visualization of skin penetration using confocal laser scanning microscopy. *European Journal of Pharmaceutics and Biopharmaceutics*, Vol. 58, pp. 301–316.

Bortner, C. D., & Cidlowski, J. A. (2002). News and Commentary Apoptotic volume decrease and the incredible shrinking cell. *Cell Death and Differentiation*, *9*, 1307–1310.

Boutin, M. E., & Hoffman-Kim, D. (2015). Application and assessment of optical clearing methods for imaging of tissue-engineered neural stem cell spheres. *Tissue Engineering - Part C: Methods*, *21*(3), 292–302.

Burg, M. B., & Ferraris, J. D. (2008, March 21). Intracellular organic osmolytes: Function and regulation. *Journal of Biological Chemistry*, Vol. 283, pp. 7309–7313.

de los Heros, P., Kahle, K. T., Rinehart, J., Bobadilla, N. A., Vá zquez, N., San Cristobal, P., … Gamba, G. (2005). *WNK3 bypasses the tonicity requirement for K-Cl cotransporter activation via a phosphatase-dependent pathway*.

Gamba, G. (2005, April). Molecular physiology and pathophysiology of electroneutral cation-chloride cotransporters. *Physiological Reviews*, Vol. 85, pp. 423–493.

Guo, M., Pegoraro, A. F., Mao, A., Zhou, E. H., Arany, P. R., Han, Y., … Weitz, D. A. (2017). Cell volume change through water efflux impacts cell stiffness and stem cell fate. *Proceedings of the National Academy of Sciences of the United States of America*, *114*(41), E8618–E8627.

Hoffmann, E. K., Lambert, I. H., & Pedersen, S. F. (2009, January). Physiology of cell volume regulation in vertebrates. *Physiological Reviews*, Vol. 89, pp. 193–277.

HOVIS, D. B., & HEUER, A. H. (2010). The use of laser scanning confocal microscopy (LSCM) in materials science. *Journal of Microscopy*, *240*(3), 173–180.

Jonkman, J., Brown, C. M., Wright, G. D., Anderson, K. I., & North, A. J. (2020, May 1). Tutorial: guidance for quantitative confocal microscopy. *Nature Protocols*, Vol. 15, pp. 1585–1611.

Kahle, K. T., Khanna, A. R., Alper, S. L., Adragna, N. C., Lauf, P. K., Sun, D., & Delpire, E. (2015). K-Cl cotransporters, cell volume homeostasis, and neurological disease. *Trends in Molecular Medicine*.

Kahle, K. T., Rinehart, J., & Lifton, R. P. (2010, December). Phosphoregulation of the Na-K-2Cl and K-Cl cotransporters by the WNK kinases. *Biochimica et Biophysica Acta - Molecular Basis of Disease*, Vol. 1802, pp. 1150–1158.

Kahle, K. T., Ring, A. M., & Lifton, R. P. (2008). Molecular Physiology of the WNK Kinases. *Annual Review of Physiology*, *70*(1), 329–355.

Kahle, K. T., Rinehart, J., De Los Heros, P., Louvi, A., Meade, P., Vazquez, N., … Lifton, R. P. (2005). WNK3 modulates transport of Cl- in and out of cells: Implications for control of cell volume and neuronal excitability. *Proceedings of the National Academy of Sciences of the United States of America*, *102*(46), 16783–16788.

Kay, A. R., & Blaustein, M. P. (2019). Evolution of our understanding of cell volume regulation by the pump-leak mechanism. *Journal of General Physiology*, *151*(4), 407–416.

Keller, P. J., & Dodt, H. U. (2012, February 1). Light sheet microscopy of living or cleared specimens. *Current Opinion in Neurobiology*, Vol. 22, pp. 138–143.

Lang, F. (2007). Mechanisms and Significance of Cell Volume Regulation. *Journal of the American College of Nutrition*, *26*(sup5), 613S-623S.

Lang, F., Föller, M., Lang, K., Lang, P., Ritter, M., Vereninov, A., … Gulbins, E. (2007). Cell Volume Regulatory Ion Channels in Cell Proliferation and Cell Death. In *Methods in Enzymology* (Vol. 428, pp. 209–225).

Lang, F., & Hoffmann, E. K. (2013, December). CrossTalk proposal: Cell volume changes are an essential step in the cell death machinery. *Journal of Physiology*, Vol. 591, pp. 6119–6121.

Larson, A. M. (2011). Multiphoton microscopy. *Nature Photonics*, *5*(1), 1–1.

Lazzari, G., Vinciguerra, D., Balasso, A., Nicolas, V., Goudin, N., Garfa-Traore, M., … Mura, S. (2019). Light sheet fluorescence microscopy versus confocal microscopy: in quest of a suitable

tool to assess drug and nanomedicine penetration into multicellular tumor spheroids. *European Journal of Pharmaceutics and Biopharmaceutics*, *142*, 195–203.

Leary, E., Rhee, C., Wilks, B. T., & Morgan, J. R. (2018). Quantitative Live-Cell Confocal Imaging of 3D Spheroids in a High-Throughput Format. *SLAS Technology*, *23*(3), 231–242.

Lee, H. P., Gu, L., Mooney, D. J., Levenston, M. E., & Chaudhuri, O. (2017). Mechanical confinement regulates cartilage matrix formation by chondrocytes. *Nature Materials*, *16*(12), 1243–1251.

Lee, H. pyo, Stowers, R., & Chaudhuri, O. (2019). Volume expansion and TRPV4 activation regulate stem cell fate in three-dimensional microenvironments. *Nature Communications*, *10*(1).

Maes, M., Crespo Yanguas, S., Willebrords, J., & Vinken, M. (2015, December 25). Models and methods for in vitro testing of hepatic gap junctional communication. *Toxicology in Vitro*, Vol. 30, pp. 569–577.

Maeno, E., Takahashi, N., & Okada, Y. (2006). Dysfunction of regulatory volume increase is a key component of apoptosis. *FEBS Letters*, *580*(27), 6513–6517.

Mongin, A. A., & Orlov, S. N. (2001). Mechanisms of cell volume regulation and possible nature of the cell volume sensor. *Pathophysiology*, *8*(2), 77–88.

Pampaloni, F., Ansari, N., & Stelzer, E. H. K. (2013, April). High-resolution deep imaging of live cellular spheroids with light-sheet-based fluorescence microscopy. *Cell and Tissue Research*, Vol. 352, pp. 161–177.

Sachs, F., & Sivaselvan, M. V. (2015). Cell volume control in three dimensions: Water movement without solute movement. *Journal of General Physiology*, *145*(5), 373–380.

Santi, P. A. (2011). Light sheet fluorescence microscopy: A review. *Journal of Histochemistry and Cytochemistry*, Vol. 59, pp. 129–138.

Stegemann, J. P., & Nerem, R. M. (2003). Altered response of vascular smooth muscle cells to exogenous biochemical stimulation in two- and three-dimensional culture. *Experimental Cell Research*.

Strange, K. (2004). Cellular volume homeostasis. *American Journal of Physiology - Advances in Physiology Education*, *28*(4), 155–159.

Tauer, U. (2002). Advantages and Risks of Multiphoton Microscopy in Physiology. *Experimental Physiology*, *87*(6), 709–714.

Toft-Bertelsen, T. L., Larsen, B. R., & MacAulay, N. (2018). Sensing and regulation of cell volume – We know so much and yet understand so little: TRPV4 as a sensor of volume changes but possibly without a volume-regulatory role? *Channels*, *12*(1), 100–108.

Ustione, A., & Piston, D. W. (2011). A simple introduction to multiphoton microscopy. *Journal of Microscopy*, *243*(3), 221–226.

Weber, M., Mickoleit, M., & Huisken, J. (2014). Light sheet microscopy. In *Methods in Cell Biology* (Vol. 123, pp. 193–215).

Williams, R. M., Zipfel, W. R., & Webb, W. W. (2001). Multiphoton microscopy in biological research. *Current Opinion in Chemical Biology*, *5*(5), 603–608.